Production of bottomonia states in proton-proton and heavy ion collisions

Vineet Kumar[d,*], Prashant Shukla[d,f], Abhijit Bhattacharyya[e]

[a]*Nuclear Physics Division, Bhabha Atomic Research Centre, Mumbai 400085, India*
[b]*Department of Physics, University of Calcutta, 92, A. P. C. Road Kolkata-700009, India*
[c]*Homi Bhabha National Institute, Anushakti Nagar, Mumbai 400094, India*

Abstract

This work reviews the study of bottomonia production in high energy hadronic collisions to investigate the fundamental aspects of Quantum Chromodynamics. Emphasis is given to the lessons learnt from the LHC data, which are reviewed in a global prospective with the results from the RHIC at lower energies used for comparison. The review covers bottomonia production in proton-proton, proton-nucleus and nucleus-nucleus collisions and includes discussion of the effects of hot and cold strongly interacting matter.

Keywords: Beauty, Quarkonium, Hadron Collision, Heavy-Ion Collision, Quark-Gluon Plasma, LHC, RHIC

Contents

*Corresponding author
Email address: vineetk@barc.gov.in (Vineet Kumar)

Production of bottomonia states in proton-proton and heavy ion collisions

Vineet Kumar[d,*], Prashant Shukla[d,f], Abhijit Bhattacharyya[e]

[d]*Nuclear Physics Division, Bhabha Atomic Research Centre, Mumbai 400085, India*
[e]*Department of Physics, University of Calcutta, 92, A. P. C. Road Kolkata-700009, India*
[f]*Homi Bhabha National Institute, Anushakti Nagar, Mumbai 400094, India*

1. Introduction

It is expected that strongly-interacting matter shows qualitatively new behavior at temperatures and/or densities which are comparable to or larger than the typical hadronic scale. It has been argued that under such extreme conditions deconfinement of quarks and gluons should set in and the thermodynamics of strongly-interacting matter could then be understood in terms of these elementary degrees of freedom. This new form of matter is called quark-gluon plasma [1, 2], or QGP. The existence of such a transition has indeed been demonstrated from first principles using Monte Carlo simulations of lattice QCD. The deconfinement transition and the properties of hot, strongly-interacting matter can be studied experimentally in heavy-ion collisions [3]. A significant part of the extensive experimental heavy-ion program is dedicated to measuring quarkonium yields since Matsui and Satz suggested that quarkonium suppression could be a signature of deconfinement [4].

In fact, the observation of anomalous suppression was considered to be a key signature of deconfinement at SPS energies [5].

2. Bottomonia production mechanism in p-p collisions

In general one can subdivide the quarkonia production process into two major parts

1. Production of a heavy quark pair in hard collisions.
2. Formation of quarkonia out of the two heavy quarks.

First process can be calculated by the perturbative QCD calculations while the formation of quarkonia out of the two heavy quarks is a non perturbative process and require some effective theories for modelling.

*Corresponding author
Email address: vineetk@barc.gov.in (Vineet Kumar)

2.1. Production of a heavy quark pair in hard collisions

Due to the high mass of the heavy quarks ($m_c \sim 1.3$ GeV/c^2, $m_b \sim 4.7$ GeV/c^2), they can be produced only during the first phase of a collision. Only at that time the elementary collisions with sufficiently high momentum transfers (to create such high masses) takes place. For this reason the heavy quark production is a hard process that can be treated perturbatively. The hadronic cross section in pp collisions can be written as

$$\sigma_{pp}(s, m^2) = \sum_{i,j=q,\bar{q},g} \int dx_1\, dx_2\, f_i^p(x_1, \mu_F^2)\, f_j^p(x_2, \mu_F^2)\, \widehat{\sigma}_{ij}(s, m^2, \mu_F^2, \mu_R^2) \quad (1)$$

where x_1 and x_2 are the fractional momenta carried by the colliding partons and f_i^p are the proton parton densities. The total partonic cross section has been completely calculated up to NLO [6, 7]. The partonic cross section is given by

$$\begin{aligned} \widehat{\sigma}_{ij}(s, m, \mu_F^2, \mu_R^2) &= \frac{\alpha_s^2(\mu_R^2)}{m^2} \left\{ f_{ij}^{(0,0)}(\rho) \right. \\ &+ \left. 4\pi\alpha_s(\mu_R^2) \left[f_{ij}^{(1,0)}(\rho) + f_{ij}^{(1,1)}(\rho) \ln\left(\frac{\mu_F^2}{m^2}\right) \right] + \mathcal{O}(\alpha_s^2) \right\} \end{aligned} \quad (2)$$

where $\rho = 4m^2/s$ and $f_{ij}^{(k,l)}$ are the scaling functions to NLO [6, 7]. At small ρ, the $\mathcal{O}(\alpha_s^2)$ and $\mathcal{O}(\alpha_s^3)$ $q\bar{q}$ and the $\mathcal{O}(\alpha_s^2)$ gg scaling functions become small while the $\mathcal{O}(\alpha_s^3)$ gg and qg scaling functions plateau at finite values. Thus, at collider energies, the total cross sections are primarily dependent on the small x parton densities and phase space. The total cross section does not depend on any kinematic variables, only on the quark mass, m, and the renormalization and factorization scales with central value $\mu_{R,F} = \mu_0 = m$.

2.2. Formation of quarkonia out of the two heavy quarks

The nonperturbative evolution of the $Q\bar{Q}$ pair into a quarkonium has been discussed extensively in terms of models and in terms of the language of effective theories of QCD [8, 9]. Different treatments of this evolution have led to various theoretical models for inclusive quarkonium production. Most notable among these are the color-singlet model (CSM), the color-evaporation model (CEM) and the non-relativistic QCD (NRQCD) factorization approach. In this review we will mainly discuss the NRQCD approach, as theoretically, it is the most modern and acceptable one. However, we will touch upon CSM and CEM briefly.

2.2.1. The color singlet model:

The CSM was first proposed shortly after the discovery of the J/ψ [10, 11, 12, 13]. In this model, it is assumed that the $Q\bar{Q}$ pair that evolves into the quarkonium is in a color-singlet state and that it has the same spin and angular-momentum quantum numbers as the quarkonium. In the CSM, the production rate

for each quarkonium state is related to the absolute values of the color-singlet $Q\bar{Q}$ wave function and its derivatives, evaluated at zero $Q\bar{Q}$ separation. These quantities can be extracted by comparing theoretical expressions for quarkonium decay rates in the CSM with experimental measurements. Once this extraction has been carried out, the CSM has no free parameters. The CSM was successful in predicting quarkonium production rates at relatively low energy [14]. Recently, it has been found that, at high energies, very large corrections to the CSM appear at next-to-leading order (NLO) and next-to-next-to-leading order (NNLO) in α_s [15, 16, 17]. Consequently, the possibility that the CSM might embody an important production mechanism at high energies has re-emerged. However, given the very large corrections at NLO and NNLO, it is not clear that the perturbative expansion in α_s is convergent. The NRQCD factorization approach encompasses the color-singlet model, but goes beyond it.

2.2.2. The color evaporation model:

The CEM [18, 19, 20] is motivated by the principle of quark-hadron duality. In the CEM, it is assumed that every produced $Q\overline{Q}$ pair evolves into a quarkonium if it has an invariant mass that is less than the threshold for producing a pair of open-flavor heavy mesons. It is further assumed that the nonperturbative probability for the $Q\overline{Q}$ pair to evolve into a quarkonium state H is given by a constant F_H that is energy-momentum and process independent. Once F_H has been fixed by comparison with the measured total cross section for the production of the quarkonium H, the CEM can predict, with no additional free parameters, the momentum distribution of the quarkonium production rate. The CEM predictions provide good descriptions of the CDF data for J/ψ, $\psi(2S)$, and χ_c production at $\sqrt{s} = 1.8$ TeV [20].

The heavy quark production cross section are calculated to NLO in pQCD using the CT10 parton densities [21]. The mass and scale parameters used for open and hidden heavy flavor production are obtained by fitting the energy dependence of open heavy flavor production to the measured total cross sections [22**?**]. Those obtained for open charm are $m_c = 1.27 \pm 0.09$ GeV, $\mu_F/m_{T\,c} = 2.10^{+2.55}_{-0.85}$, and $\mu_R/m_{T\,c} = 1.60^{+0.11}_{-0.12}$ [22]. The botttom quark mass and scale parameters are $m_b = 4.65 \pm 0.09$ GeV, $\mu_F/m_{T\,b} = 1.40^{+0.75}_{-0.47}$, and $\mu_R/m_{T\,b} = 1.10^{+0.26}_{-0.19}$ [**?**]. The quarkonium production cross sections are calculated in the color evaporation model with normalizations determined from fitting the scale parameter to the shape of the energy-dependent cross sections [22**?**]. The resulting uncertainty bands are smaller than those obtained with the fiducial parameters used in Ref. [23]. We note that the new results are within the uncertainties of those Ref. [23]. Indeed, the charm cross sections reported at the LHC agree better with the new values of the mass and scale than the central value of $m_c = 1.5$ GeV, $\mu_F/m_T = \mu_R/m_T = 1$.

Table 1: Heavy quark and quarkonia production cross sections at $\sqrt{s_{_{NN}}} = 2.76$ TeV. The cross sections are given per nucleon pair while $N^{\rm PbPb}$ gives the initial number of heavy quark pair/quarkonia per Pb+Pb event.

	$c\bar{c}$	J/ψ	$b\bar{b}$	Υ
σ_{pp}	$4.11^{+2.69}_{-2.50}$ mb	$21.6^{+10.6}_{-10.4}$ μb	$110.5^{+15.1}_{-14.2}$ μb	$0.22^{+0.07}_{-0.06}$ μb
$\sigma_{\rm PbPb}$	$3.21^{+2.1}_{-1.95}$ mb	$16.83^{+8.26}_{-8.10}$ μb	$100.5^{+13.7}_{-12.9}$ μb	$0.199^{+0.063}_{-0.054}$ μb
$N^{\rm PbPb}$	18.12^{+12}_{-11}	$0.0952^{+0.047}_{-0.046}$	$0.57^{+0.08}_{-0.07}$	$0.001123^{+0.0004}_{-0.0003}$

The central EPS09 NLO parameter set [24] is used to calculate the modifications of the parton distribution functions (nPDF) in Pb+Pb collisions, referred as cold nuclear matter (CNM) effects. The CNM uncertainty is calculated by adding the EPS09 NLO uncertainties in quadrature.The production cross sections for heavy flavor and quarkonia at $\sqrt{s_{_{NN}}}$ = 2.76 TeV [25] are given in Table 1. The yields in a minimum bias Pb+Pb event is obtained from the per nucleon cross section, $\sigma_{\rm PbPb}$, in Table 1, as

$$N = \frac{A^2 \sigma_{\rm PbPb}}{\sigma^{\rm tot}_{\rm PbPb}} \ . \tag{3}$$

At 2.76 TeV, the total Pb+Pb cross section, $\sigma^{\rm tot}_{\rm PbPb}$, is 7.65 b [26].

2.2.3. The NRQCD factorization approach:

Quantum Chromodynamics (QCD) describes the strong interaction among the quarks and gluons via perturbative calculations utilising its property called asymptotic freedom. On the other hand, these quarks and gluons are confined inside hadrons which are the colour singlet states. Confinement is a purely non-perturbative phenomenon which is not very well understood yet. The study of quarkonia ($Q\bar{Q}$) serves as an effective tool to look at both of these perturbative and non-perturbative aspects of QCD. The quarkonia states differ from most other hadrons due to the small velocity, v of the massive constituents and thus can be treated using non-relativistic formalism [27, 28]. In a simple picture, one can think of a quarkonium as a heavy quark pair ($Q\bar{Q}$) bound in a colour singlet state by some effective potential interaction, where the constituents are separated by distances much smaller than $1/\Lambda_{\rm QCD}$ where $\Lambda_{\rm QCD}$ is the QCD scale. This interaction gets screened in the presence of a deconfined medium like Quark Gluon Plasma (QGP), causing the bound state to melt away and thus the quarkonia yields are suppressed in the heavy ion collisions. This makes quarkonia an important probe of QGP. However cold nuclear matter effects such as modification of parton distribution functions of nucleons inside nucleus also affect their yields. There have been immense experimental [29, 30, 31, 32] and theoretical works [33, 34, 35, 36] on quarkonia modifications in PbPb collisions for which understanding of quarkonia production in pp collisions is an important prerequisite.

The massive quarks (with $m_c \sim 1.6$ GeV/c^2, $m_b \sim 4.5$ GeV/c^2) are produced in initial stages in hadronic collision with high momentum transfer and thus can be treated perturbatively [7]. The emergence of quarkonia out of the two massive quarks, on the other hand can only be described non-perturbatively using different models [8, 37]. The Colour Singlet Model (CSM) [10, 13], Colour Evaporation Model (CEM) [18, 19], the Fragmentation Scheme and the NRQCD factorisation formalism are some of the well established models for quarkonia production. In the framework of CSM, the $Q\bar{Q}$ pair, eventually evolving into the quarkonium, is assumed to be in Colour Singlet (CS) state and that has spin and angular momentum same as that of quarkonium. Apart from comprising of the CSM, the NRQCD factorisation approach incorporates the Colour Octet (CO) states as well.

In the formalism of the NRQCD factorisation approach, the evolution probability of $Q\bar{Q}$ pair into a state of quarkonium is expressed as matrix elements of NRQCD operators expanded in terms of heavy quark velocity v (for $v \ll 1$) [8]. The factorisation formulae were then used to calculate production cross-sections and decay rates of quarkonia states. The full structure of the $Q\bar{Q}$ Fock space is considered and spanned by $n{=}^{2s+1}L_J^{[a]}$ state where s is the spin, L is the orbital angular momentum, J is the total angular momentum and a (colour multiplicity) = 1 for CS and 8 for CO states. The produced CO states of $Q\bar{Q}$ pair at short distances emerge as CS quarkonia by emitting soft gluons non-perturbatively. The short distance cross-sections are obtained theoretically using methods of perturbative QCD (pQCD). The long distance matrix elements (LDME) that correspond to the probability of $Q\bar{Q}$ pair to emerge as quarkonium are extracted by fitting the measured cross-section data.

There have been several works on bottomonia production based on NRQCD formalism. In Ref. [38], a Monte Carlo framework has first been employed with CO mechanism for inclusive bottomonia production and few NRQCD CO matrix elements for Υ(1S) have been extracted at the Tevatron energy. The study has been extended to the whole Υ(nS) family in Ref. [39] to find CO matrix elements using CDF measurements at Tevatron. In Ref. [**?**] the CO matrix elements are obtained for Υ(nS) family and the feed downs from χ_b(1P) and χ_b(2P) to Υ(1S) have been considered. In Ref. [40], the Υ production has been obtained via S-wave CO states calculated at Next to Leading Order (NLO). The LDMEs are obtained by fitting the Tevatron data. The ratios of NLO to LO total cross-sections have been obtained at Tevatron and LHC energies. Polarisation of inclusive Υ has been obtained albeit with large uncertainties. In Ref. [41] both CS and CO states along with feed down contributions from higher states have been considered to study the quarkonia yields for RHIC and LHC energies. Using Collins-Soper-Sterman (CSS) formalism, an

extension of the NRQCD prediction has been carried forward for heavy quarkonium production at low p_T by considering soft gluon resummation at all orders in Ref. [42].

Both production and polarisation of Υ(nS) at NLO have been discussed in Ref. [43] within the framework of NRQCD. The CO matrix elements are obtained by fitting with experimental data. The study is updated in Ref. [44] by considering feed down from χ_{bJ}(mP) states in Υ(nS) production. The yields and polarisations of Υ(nS) measured at Tevatron and LHC are well explained by this work. The NLO study in Ref. [45] describes the yields and polarisations of Υ(nS) at LHC which includes feed down contributions from higher states. In Ref. [46], production cross-section for Υ(nS), χ_{bJ}, η_b and h_b have been calculated using NRQCD, as produced in hard photo production and fragmentation processes at LHC energies.

A LO NRQCD analyis is useful as it is straightforward and unique and once the parameters are obtained by fitting over large datasets it has excellent predictability power for unknown cross sections. The short distance QCD cross-sections calculation techniques at NLO are not unique. Moreover the different components of pQCD NLO cross sections are not available in public domain. Many NLO analysis do not include the feed down contribution from the higher states. It is shown that there is a large difference amoung the LDMEs obtained by different analysis at NLO. In this paper, the LO NRQCD calculations for the differential production cross-sections of Υ states in p+p collisions have been presented. The NRQCD formalism is described briefly in Section 2.2.3. A large set of data from Tevatron [47] and LHC [48, 49, 50, 51, 52] is used to extract the LDMEs required for the Υ production and then results are presented in Section 2.2.3. A comparison of the obtained LDMEs with the previous NRQCD studies both at LO and NLO has been made. The summary of our findings are discussed in Section 2.2.3. An updated QCD LO study on the bottomonia hadroproduction is useful as it provides a reference for comparison with NLO calculations.

Bottomonia production in p+p collisions. In order to study heavy quarkonium yield, the NRQCD framework serves as an efficient theoretical tool. The processes that govern the differential production of heavy mesons like bottomonium, as functions of p_T are mostly 2→2 operations. These processes can be denoted generically by $a+b \rightarrow \Upsilon + X$, where a and b are the incident light partons, Υ is the heavy meson and X is final state light parton. The double differential cross-section as a function of p_T and rapidity (y) of the heavy meson can be written as [54],

$$\begin{aligned} \frac{d^2\sigma^{\Upsilon}}{dp_T dy} &= \sum_{a,b} \int_{x_a^{min}}^{1} dx_a G_{a/p}(x_a, \mu_F^2) G_{b/p}(x_b, \mu_F^2) \\ &\times 2p_T \frac{x_a x_b}{x_a - \frac{m_T}{\sqrt{s}} e^y} \frac{d\sigma}{d\hat{t}} \end{aligned} \tag{4}$$

where, $G_{a/p}(G_{b/p})$ are the colliding parton $(a(b))$ distribution functions in the incident protons. They depend on the fractions $x_a(x_b)$, of the total momentum carried by the incident partons and the scale of factorisation μ_F. Here $\sqrt{s}$ represents the total center of mass energy of the pp system and m_T $(= \mu_F)$ stands for the transverse mass,

Table 2: Necessary and pertinent branching fractions for bottomonia family [45, 53].

Meson from	Meson to								
	Υ(3S)	χ_{b0}(2P)	χ_{b1}(2P)	χ_{b2}(2P)	Υ(2S)	χ_{b0}(1P)	χ_{b1}(1P)	χ_{b2}(1P)	Υ(1S)
χ_{b0}(3P)	0.005				0.002				0.002
χ_{b1}(3P)	0.104				0.037				0.038
χ_{b2}(3P)	0.061				0.019				0.019
Υ(3S)		0.131	0.126	0.059	0.199	0.003	0.0017	0.019	0.066
χ_{b0}(2P)					0.014				0.004
χ_{b1}(2P)					0.199				0.092
χ_{b2}(2P)					0.106				0.070
Υ(2S)						0.038	0.0715	0.069	0.260
χ_{b0}(1P)									0.019
χ_{b1}(1P)									0.352
χ_{b2}(1P)									0.180

Table 3: CS and CO elements for Υ family, obtained theoretically/extracted using experimental data [41, 44].

Direct Contributions	Feed down contributions from higher s-wave states	Feed down contributions from higher p-wave states
$M_L(b\bar{b}([^3S_1]_1) \to \Upsilon(3S))$ =4.3 GeV^3	$M_L(b\bar{b}([^3S_1]_1) \to \Upsilon(3S, 2S))$ =4.3, 4.5 GeV^3	$M_L(b\bar{b}([^3P_0]_1) \to \chi_{b0}(1P))$ =0.100m_b^2 GeV^3
$M_L(b\bar{b}([^3S_1]_1) \to \Upsilon(2S))$ =4.5 GeV^3	$M_L(b\bar{b}([^3S_1]_8) \to \Upsilon(3S, 2S))$	$M_L(b\bar{b}([^3S_1]_8) \to \chi_{b0}(1P))$ =0.0094 GeV^3
$M_L(b\bar{b}([^3S_1]_1) \to \Upsilon(1S))$ =10.9 GeV^3	$M_L(b\bar{b}([^1S_0]_8) \to \Upsilon(3S, 2S))$	$M_L(b\bar{b}([^3P_0]_1) \to \chi_{b0}(2P))$ =0.100m_b^2 GeV^3
$M_L(b\bar{b}([^3S_1]_8) \to \Upsilon(nS))$	$M_L(b\bar{b}([^3P_0]_8) \to \Upsilon(3S, 2S))$	$M_L(b\bar{b}([^3S_1]_8) \to \chi_{b0}(2P))$ =0.0109 GeV^3
$M_L(b\bar{b}([^1S_0]_8) \to \Upsilon(nS))$	$M_L(b\bar{b}([^3P_1]_8) \to \Upsilon(3S, 2S))$ =3$M_L(b\bar{b}([^3P_0]_8) \to \Upsilon(3S, 2S))$	$M_L(b\bar{b}([^3P_0]_1) \to \chi_{b0}(3P))$ =0.100m_b^2 GeV^3
$M_L(b\bar{b}([^3P_0]_8) \to \Upsilon(nS))$	$M_L(b\bar{b}([^3P_2]_8) \to \Upsilon(3S, 2S))$ =5$M_L(b\bar{b}([^3P_0]_8) \to \Upsilon(3S, 2S))$	$M_L(b\bar{b}([^3S_1]_8) \to \chi_{b0}(3P))$ =0.0069 GeV^3
$M_L(b\bar{b}([^3P_1]_8) \to \Upsilon(nS))$ 3$M_L(b\bar{b}([^3P_0]_8) \to \Upsilon(nS))$		
$M_L(b\bar{b}([^3P_2]_8) \to \Upsilon(nS))$ 5$M_L(b\bar{b}([^3P_0]_8) \to \Upsilon(nS))$		

$m_T^2 = p_T^2 + M^2$ of the quarkonium. The relation between x_a and x_b and the expression for x_a^{min} are given in our earlier work [54]. The $d\sigma/d\hat{t}$ in Eq. 4 is the parton level cross-section and is defined as [8],

$$\frac{d\sigma}{d\hat{t}} = \frac{d\sigma}{d\hat{t}}(ab \to Q\bar{Q}(^{2s+1}L_J) + X) M_L(Q\bar{Q}(^{2s+1}L_J) \to \Upsilon) \tag{5}$$

The first term in RHS is the short distance contribution, that corresponds to the $Q\bar{Q}$ pair production in specific colour and spin configuration and is calculable using perturbative QCD (pQCD) [**?** 55, 56, 57, 58, 59]. The other term in the RHS of Eq.(5) is the Long Distance Matrix Element (LDME) and refers to the probability of the $Q\bar{Q}$ state to convert into a quarkonium state. They are determined by contrasting with experimental observations.

The NRQCD formalism provides an adequate procedure to estimate a quantity as an expansion in heavy quark relative velocity, v inside $Q\bar{Q}$ bound state. The LDME in Eq.(5) do scale with definitive power in v. The quarkonium yield depends on the $^3S_1^{[1]}$ and $^3P_J^{[1]}$(J=0,1,2) CS states and $^1S_0^{[8]}$, $^3S_1^{[8]}$ and $^3P_J^{[8]}$ CO states in the limit $v \ll 1$. The superscripts in square brackets represent the colour structure of the bound state, 1 for the CS and 8 for the CO. The direct production cross-section for Υ in differential form can thus be expressed as the sum of all contributions,

$$\begin{aligned}
d\sigma(\Upsilon(nS)) &= d\sigma(Q\overline{Q}([^3S_1]_1)) M_L(Q\bar{Q}([^3S_1]_1) \to \Upsilon(nS)) \\
&+ d\sigma(Q\overline{Q}([^1S_0]_8)) M_L(Q\bar{Q}([^1S_0]_8) \to \Upsilon(nS)) \\
&+ d\sigma(Q\overline{Q}([^3S_1]_8)) M_L(Q\bar{Q}([^3S_1]_8) \to \Upsilon(nS)) \\
&+ d\sigma(Q\overline{Q}([^3P_0]_8)) M_L(Q\bar{Q}([^3P_0]_8) \to \Upsilon(nS)) \\
&+ d\sigma(Q\overline{Q}([^3P_1]_8)) M_L(Q\bar{Q}([^3P_1]_8) \to \Upsilon(nS)) \\
&+ d\sigma(Q\overline{Q}([^3P_2]_8)) M_L(Q\bar{Q}([^3P_2]_8) \to \Upsilon(nS)) \\
&+ ...
\end{aligned} \tag{6}$$

The dots include terms having contributions in higher powers of v.

The contributions from CS-$[^3P_J]_1$ and CO-$[^3S_1]_8$ states are in the same order of v for the p-wave bound states, $\chi_b(nP)$. The angular momentum barriers of the p-wave states are held responsible for that to happen and thereby making them important enough to be considered. The differential cross-section for χ_b production henceforth is given by,

$$\begin{aligned}
d\sigma(\chi_{bJ}(1P)) &= d\sigma(Q\overline{Q}([^3P_J]_1)) M_L(Q\bar{Q}([^3P_J]_1) \to \chi_{bJ}(1P)) \\
&+ d\sigma(Q\overline{Q}[^3S_1]_8)) M_L(Q\bar{Q}([^3S_1]_8) \to \chi_{bJ}(1P)) \\
&+ ...
\end{aligned} \tag{7}$$

The experimental observations of Υ production at LHC energies, not only have contributions from direct yield, but also consist of feed downs from decay of heavier bottomonia states. The corresponding branching fractions are provided in Table 2.

We require both CS and CO matrix elements in order to get theoretical predictions for the production of bottomonia at the Tevatron and LHC energies. The corresponding expressions and numerical values for CS states are obtained from Ref. [**?**]. The CO states, on the other hand, cannot be directly connected to the non-relativistic wavefunctions of heavy mesons, as these are associated with a higher Fock state. Experimentally measured data sets are therefore

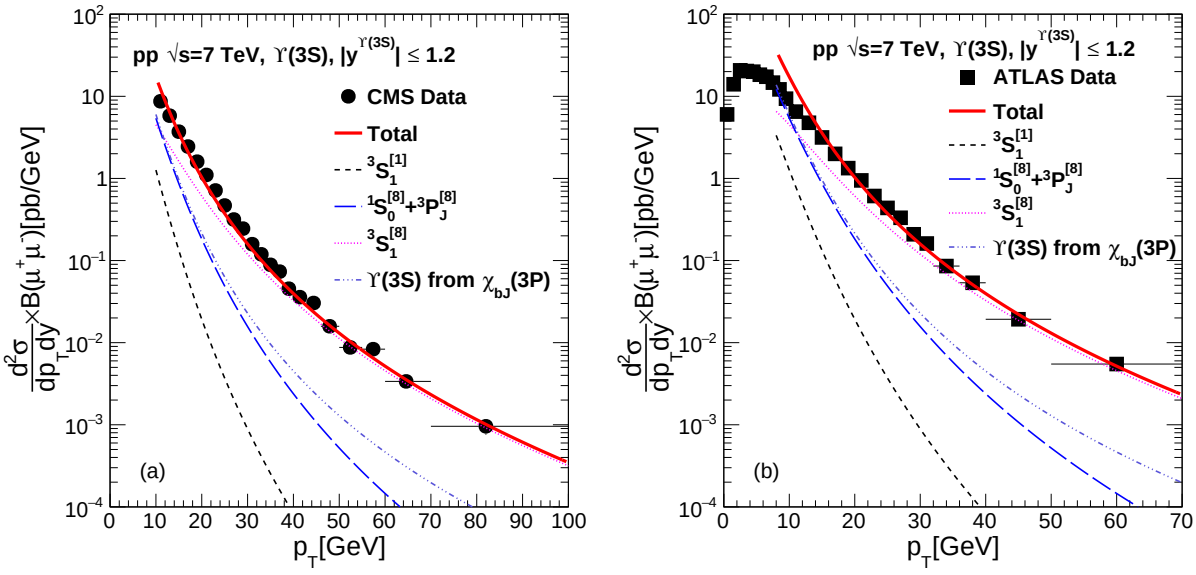

Figure 1: The NRQCD calculations of production cross-section of $\Upsilon(3S)$ in p+p collisions at $\sqrt{s}$ = 7 TeV in central rapidities, as a function of transverse momentum compared with the measured data at CMS [49] and ATLAS [50] experiment.

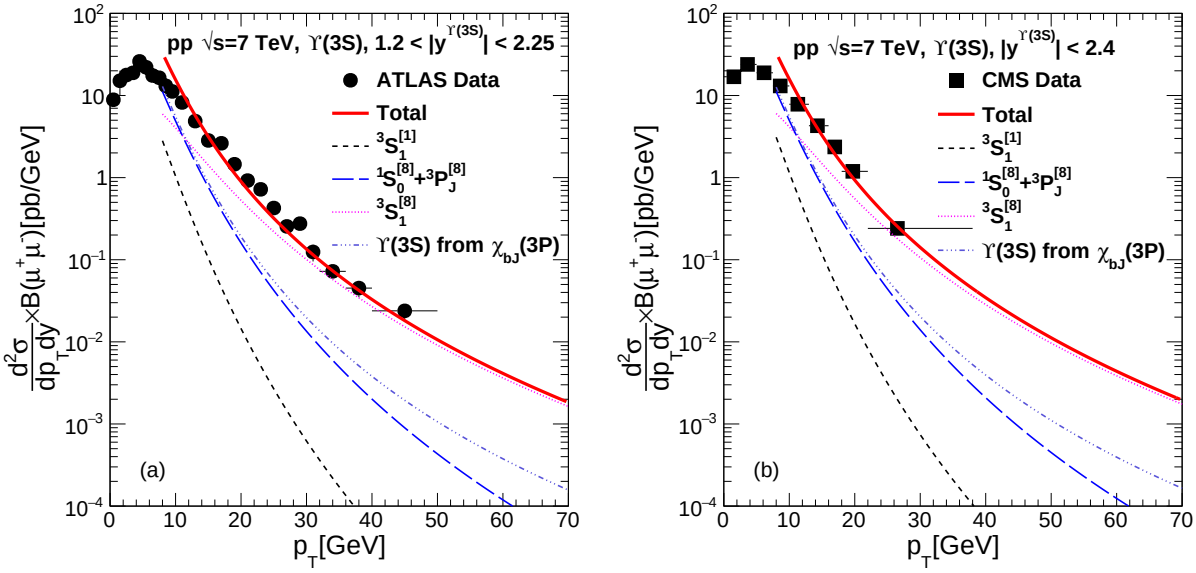

Figure 2: The NRQCD calculations of production cross-section of $\Upsilon(3S)$ in p+p collisions at $\sqrt{s}$ = 7 TeV in forward rapidities, as a function of transverse momentum compared with the measured data at ATLAS [50] and CMS [51] experiments.

employed to obtain them as in Refs. [**?** 58, 59]. The CS operators along with their theoretical values and the CO operators to be fitted are listed in Table 3, where, n=1,2,3. For the CO elements related to p-wave states, needed as the feed down contributions, we have used values obtained by Ref. [41, 44] for the present purpose. In our calculations, we have used CT18NLO parametrisation [60] for parton distribution functions and the bottom quark mass m_b is taken to be 4.88 GeV. The short distance cross-sections for $[^1S_0]_8$ and $[^3P_J]_8$ states having similar p_T dependencies, the corresponding distributions become sensitive upto a linear combination of their LDMEs. We therefore take resort to a linear combination following Ref. [54] as,

Table 4: Comparison of CS elements and CO LDMEs extracted from fitting with experimental data using NRQCD formalism for Υ(3S).

Ref. (LO/NLO)	PDF	m_b (GeV)	$M_L(b\bar{b}([^3S_1]_1 \rightarrow \Upsilon(3S)$ (GeV^3)	$M_L(b\bar{b}([^3S_1]_8 \rightarrow \Upsilon(3S)$ (GeV^3)	$M_L(b\bar{b}([^1S_0]_8, [^3P_0]_8 \rightarrow \Upsilon(3S)$ (GeV^3)	p_T-cut GeV/c
present (LO)	CT18	4.88	4.3	0.0543±0.0007	0.0097±0.0005	8
[39] (LO)	CTEQ4L	4.88	3.54	0.099±0.011	0	2
				0.091±0.015	0	4
				0.068±0.011	0	8
[**?**] (LO)	CTEQ5L	4.77	4.3±0.9	0.036±0.019	0.0108±0.0086	8
				0.039±0.017	0.0342±0.0276	
	MRSTLO	4.77	4.3±0.9	0.037±0.021	0.0150±0.0098	8
				0.041±0.019	0.0474±0.0312	
[40] (NLO)	CTEQ6M	5.18	1.128	0.03250±0.00876	0.000920±0.000968	-
[41] (LO)	MSTW08LO	4.88	4.3	0.0513±0.0085	0.0002±0.0062	-
[43] (NLO)	CTEQ6M	5.18	1.128	0.0271±0.0013	0.00956±0.00476	8
[44] (NLO)	CTEQ6M	5.18	1.128	0.0132±0.0020	-0.00520±0.00518	8

$$M_L(b\bar{b}([^1S_0]_8, [^3P_0]_8) \rightarrow \Upsilon(nS)) = \frac{M_L(b\bar{b}([^1S_0]_8) \rightarrow \Upsilon(nS))}{5} + \frac{3M_L(b\bar{b}([^3P_0]_8) \rightarrow \Upsilon(nS))}{m_b^2}.$$

Results and discussions. We first start with the production of Υ(3S) which has feed down contributions only from χ_b(3P). As described, the expressions and the values for the colour-singlet elements can be obtained by solving the non-relativistic wavefunctions [58]. The CO LDMEs on the other hand, cannot be connected to the non-relativistic wavefunctions of $b\bar{b}$. The measured data sets from different experimental collaborations are thus used to constrain them.

Figure 1 shows the NRQCD calculations of production cross-section of Υ(3S) in p+p collisions as a function of transverse momentum compared with the measured data in CMS [49] and ATLAS [50] detectors at LHC in central rapidities. In Figure 2, similar comparisons have been shown with data for $1.2 < |y| < 2.25$ and $|y| < 2.4$ measured at ATLAS [50] and CMS [51] detectors respectively. Figure 3 corresponds to CMS [52] measurements at $\sqrt{s} = 13$ TeV for rapidities, $|y| < 0.6$, $0.6 < |y| < 1.2$ and $|y| < 1.2$, whereas in Figure 4 we have used measurements from CDF [47] collaboration in p +$\bar{\text{p}}$ at $\sqrt{s} = 1.8$ TeV with $|y| < 0.4$ as well as that from LHCb [48] collaboration in p+p

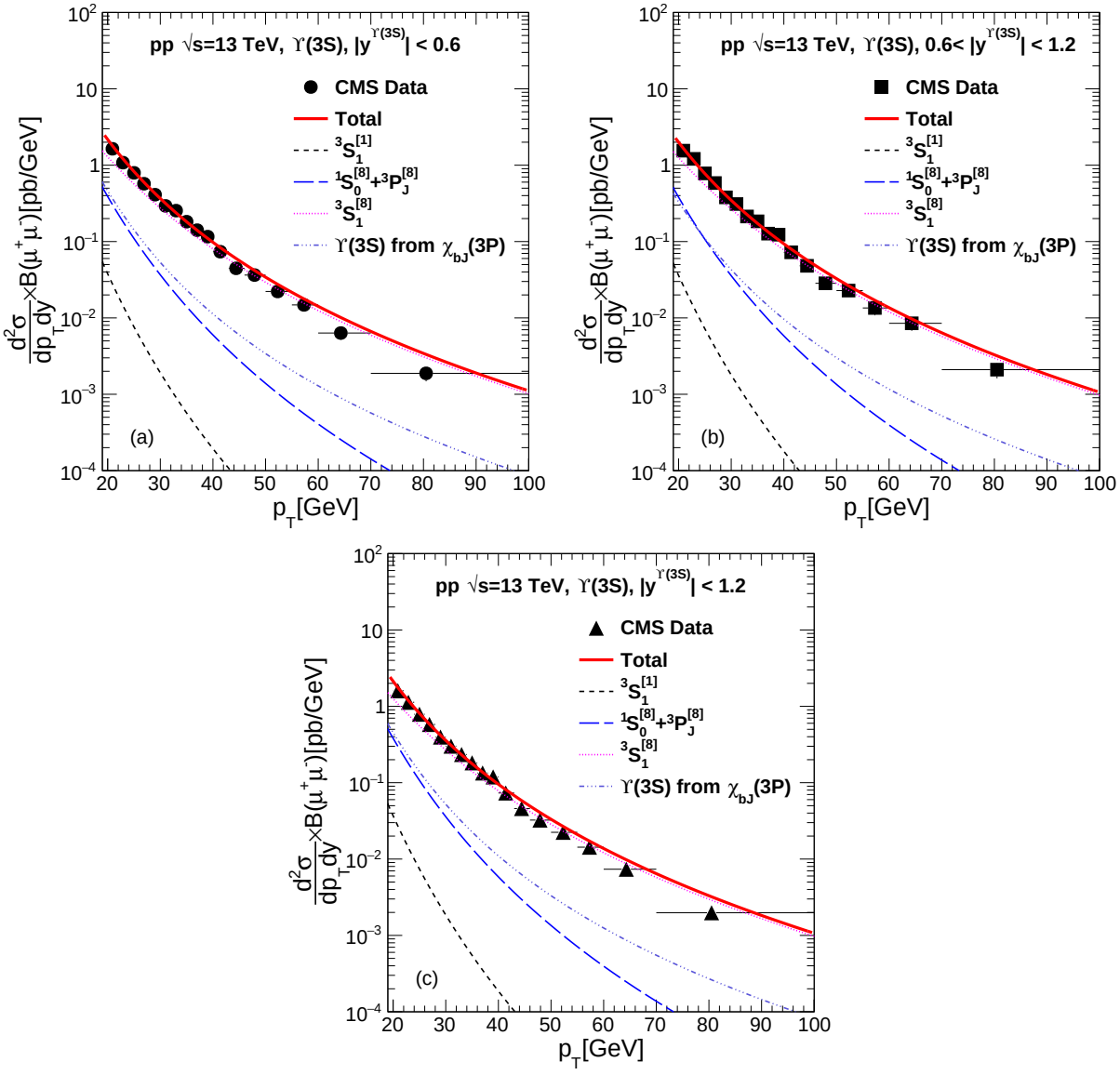

Figure 3: The NRQCD calculations of production cross-section of $\Upsilon(3S)$ in p+p collisions at $\sqrt{s}$ = 13 TeV in central and forward rapidities, as a function of transverse momentum compared with the measured data at CMS [52] experiment.

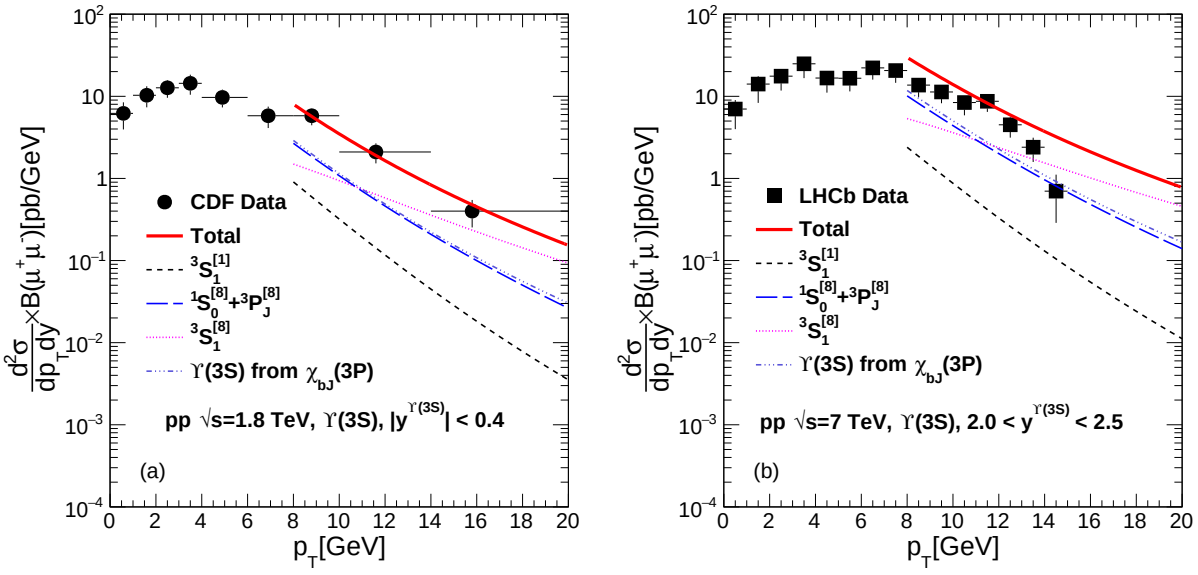

Figure 4: The NRQCD calculations of production cross-section of $\Upsilon(3S)$ in p +$\bar{\text{p}}$ collisions at $\sqrt{s}$ = 1.8 TeV and p+p collisions at 7 TeV in forward rapidities, as a function of transverse momentum compared with the measured data at CDF [47] and LHCb [48] experiment.

collisions at $\sqrt{s} = 7$ TeV with rapidities $2.0 < y < 2.5$. The LDMEs are obtained by a combined fit using all the aforesaid datasets. The χ^2/ndof is ~ 4 for the combined fitting.

Table 4 contains LDMEs for $\Upsilon(3S)$ extracted in present analysis in comparison with different other results. Our result for the matrix element $M_L(b\bar{b}([^3S_1]_8))$ shows a close proximity with LO analysis of Ref. [**?** 41], the errors being improved considerably. In our work, we have considered a linear combination of the other two colour octet LDMEs in the form of $\frac{M_L([^1S_0]_8)}{5} + \frac{3M_L([^3P_0]_8)}{m_b^2}$, same as that done in Ref. [41]. There have been different ways to treat the colour octet LDMEs in the literature. In Ref. [39], the authors have taken this combination as $M_L([^1S_0]_8) + \frac{5M_L([^3P_0]_8)}{m_b^2}$. In Ref. [**?**], these two matrix elements, $M_L([^1S_0]_8)$ and $\frac{5M_L([^3P_0]_8)}{m_b^2}$ have been extracted separately using two different PDFs. In each case however, they have extracted either of the two parameters considering the other to be vanishing. The work in Ref. [40] concentrates only on S-wave colour states. In Refs. [43, 44], the parameters, $M_L([^1S_0]_8)$ and $\frac{M_L([^3P_0]_8)}{m_b^2}$ have been extracted separately altogether. On the other hand in Ref. [45], the authors have considered different combinations of colour octet states to fit with the experimental data with NRQCD at LO and NLO using CTEQ6L1 and CTEQ6M PDFs respectively with m_b=4.75 GeV and $[^3S_1]_1$=3.54 GeV^3. Their extracted parameters are,

$$\begin{aligned} M_{0,r_0} &= [^1S_0]_8 + \frac{r_0}{m_b^2}[^3P_0]_8 = 0.0283 \pm 0.0007 \text{ GeV}^3 \\ M_{1,r_1} &= [^3S_1]_8 + \frac{r_1}{m_b^2}[^3P_0]_8 = 0.0083 \pm 0.0002 \text{ GeV}^3 \end{aligned} \tag{8}$$

with r_0=3.8 and r_1=-0.52 GeV^2.

After fixing the $\Upsilon(3S)$ yield, we next consider $\Upsilon(2S)$ production that has feed down contributions from $\Upsilon(3S)$, $\chi_b(2P)$ and $\chi_b(2P)$ states along with the direct production. The corresponding branching fractions for the feed down sectors are given in Table 2. We have used our extracted values of the $\Upsilon(3S)$ LDMEs for the feed down contributions

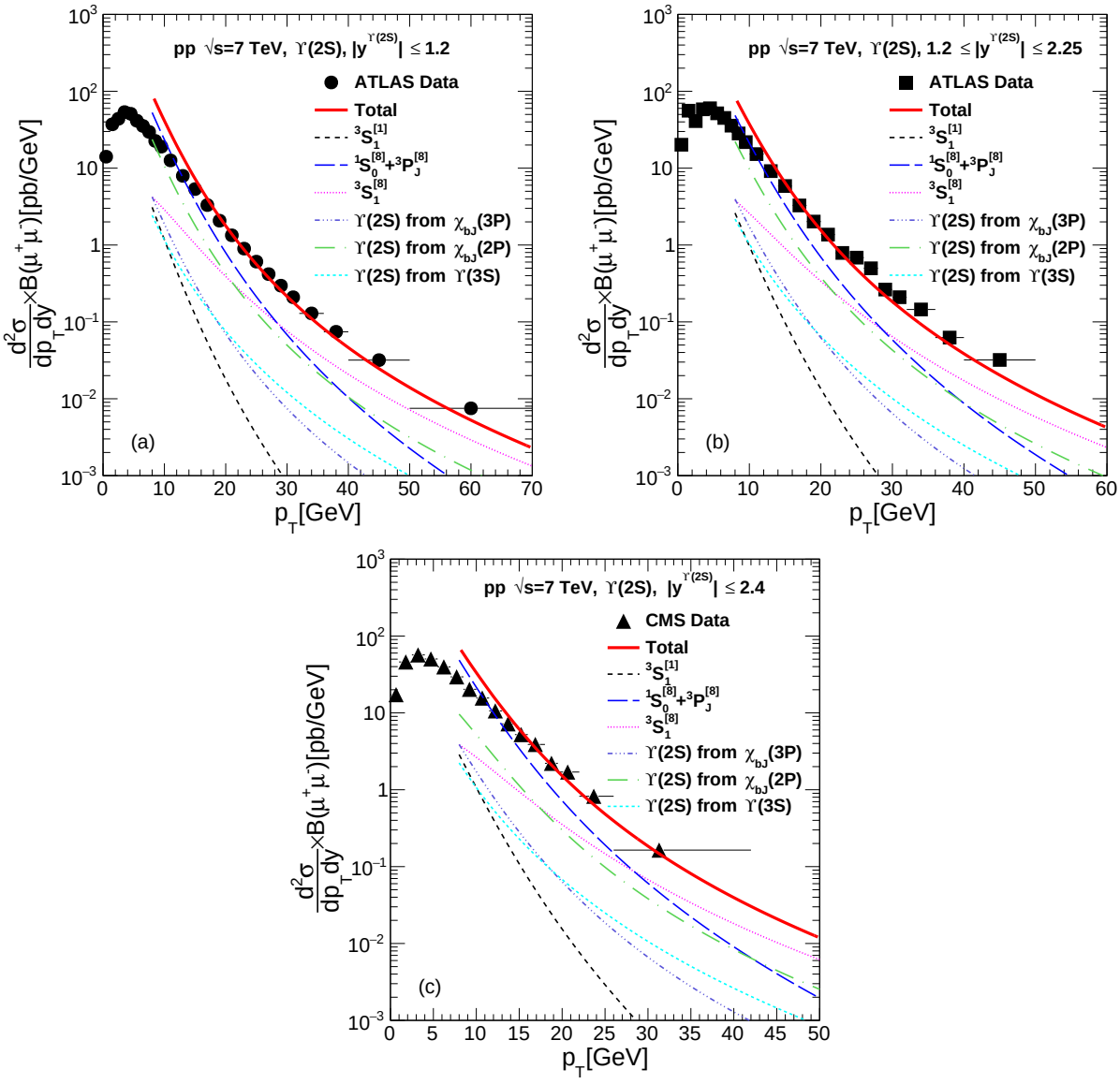

Figure 5: The NRQCD calculations of production cross-section of Υ(2S) in p+p collisions at $\sqrt{s}$ = 7 TeV in central and forward rapidities, as a function of transverse momentum compared with the measured data at CMS [51] and ATLAS [50] experiments.

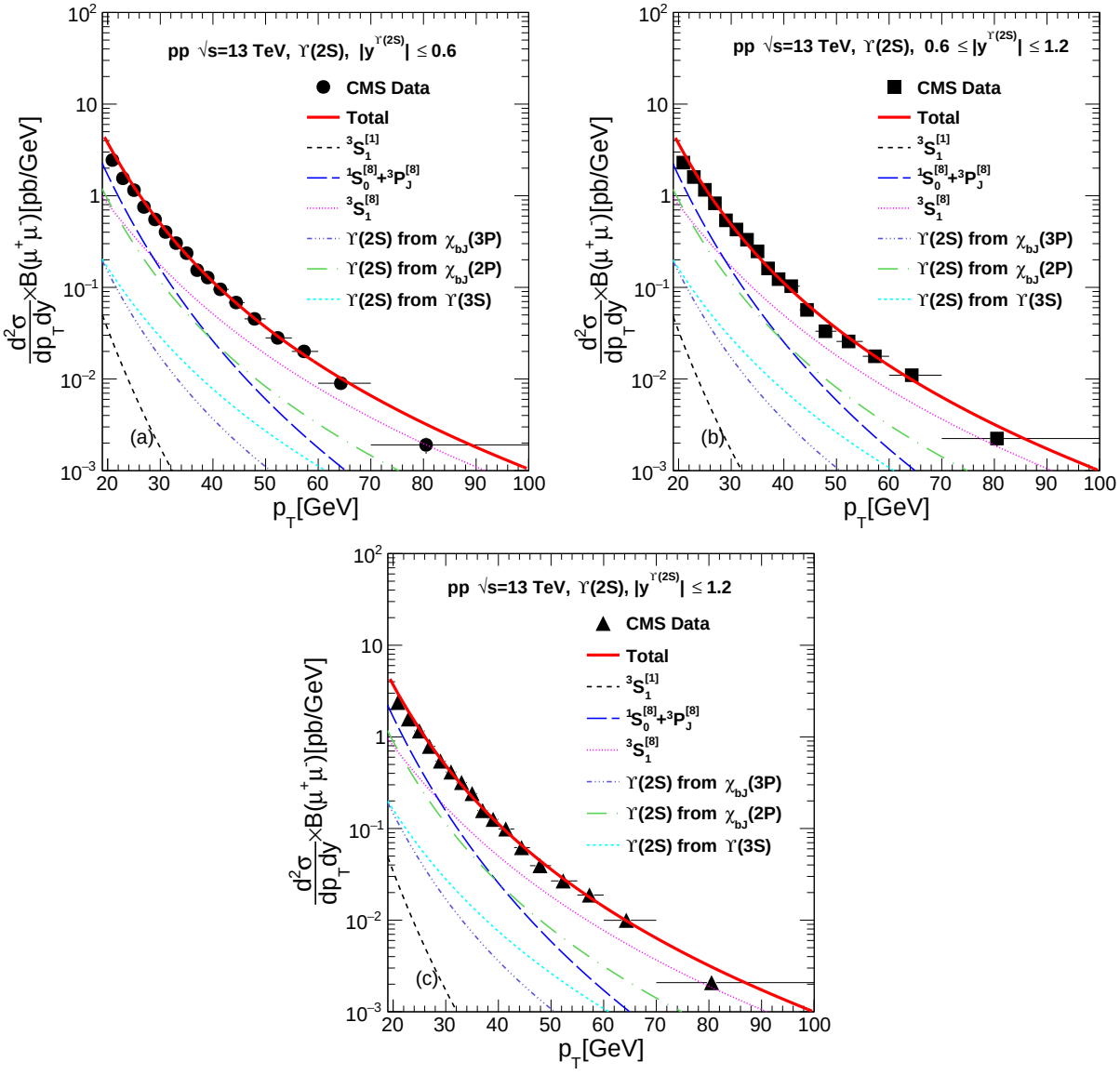

Figure 6: The NRQCD calculations of production cross-section of $\Upsilon(2S)$ in p+p collisions at $\sqrt{s}$ = 13 TeV in central and forward rapidities, as a function of transverse momentum compared with the measured data at CMS [52] experiment.

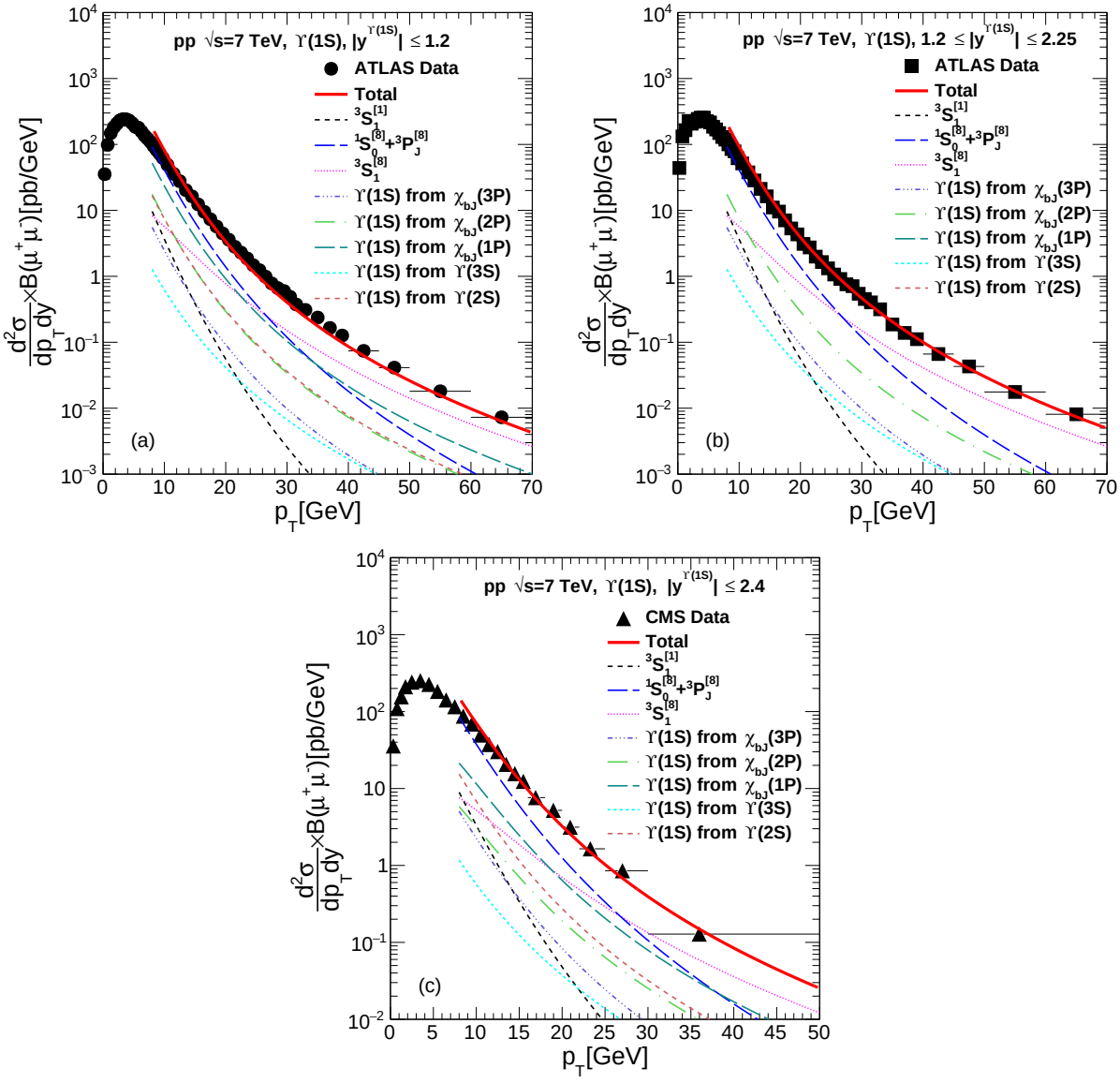

Figure 7: The NRQCD calculations of production cross-section of $\Upsilon(1S)$ in p+p collisions at $\sqrt{s}$ = 7 TeV in central and forward rapidities, as a function of transverse momentum compared with the measured data at ATLAS [50] and CMS [51] experiments.

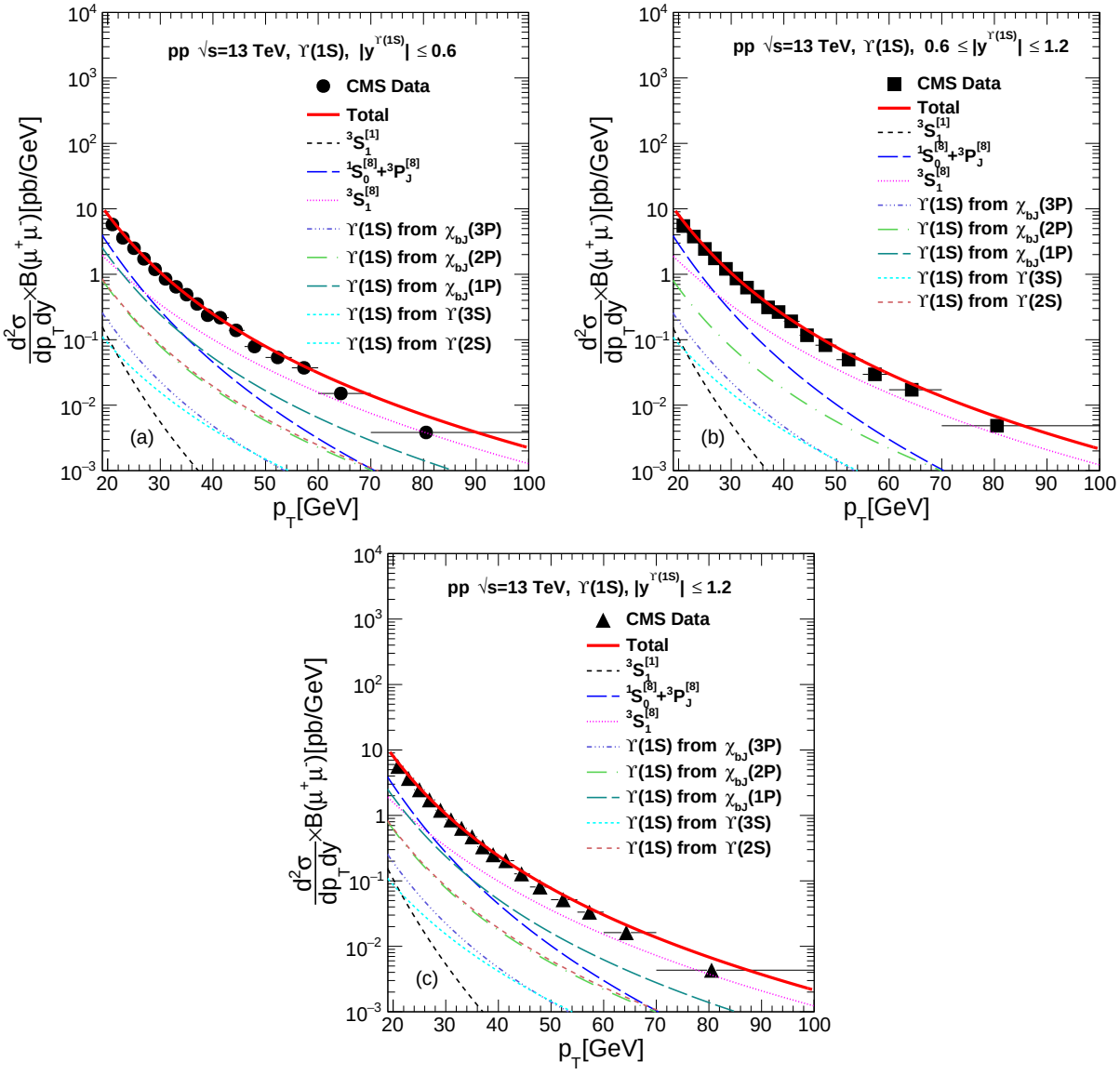

Figure 8: The NRQCD calculations of production cross-section of $\Upsilon(1S)$ in p+p collisions at $\sqrt{s}$ = 13 TeV in central and forward rapidities, as a function of transverse momentum compared with the measured data at CMS [52] experiment.

Table 5: Comparison of CS elements and CO LDMEs extracted from fitting with experimental data using NRQCD formalism for Υ(2S).

Ref. (LO/NLO)	PDF	m_b (GeV)	$M_L(b\bar{b}([^3S_1]_1 \to \Upsilon(2S)$ (GeV^3)	$M_L(b\bar{b}([^3S_1]_8 \to \Upsilon(2S)$ (GeV^3)	$M_L(b\bar{b}([^1S_0]_8, [^3P_0]_8 \to \Upsilon(2S)$ (GeV^3)	p_T-cut GeV/c
present (LO)	CT18	4.88	4.5	0.0391±0.0016	0.0477±0.0019	8
[39] (LO)	CTEQ4L	4.88	5.01	0.040±0.029	0	2
				0.073±0.018	0	4
				0.103±0.027	0	8
[**?**] (LO)	CTEQ5L	4.77	5.0±0.7	0.180±0.056	-0.102±0.097	8
				0.172±0.050	-0.106±0.102	
	MRSTLO	4.77	5.0±0.7	0.196±0.063	-0.087±0.111	8
				0.190±0.056	-0.089±0.117	
[41] (LO)	MSTW08LO	4.88	4.5	0.0224±0.0200	-0.0067±0.0084	-
[43] (NLO)	CTEQ6M	5.01	4.63	0.0030±0.0078	0.0075±0.0217	8
[44] (NLO)	CTEQ6M	5.01	4.63	0.0222±0.0024	-0.0003±0.0203	8

from the Υ(3S). To include the $\chi_b(nP)$ states feed down LDMEs are obtained from Ref. [41, 44].

In Fig 5, we have shown our NRQCD predictions of production cross-sections for Υ(2S) in p+p collisions as functions of p_T along with the measured data in CMS [51] and ATLAS [50] detectors at central and forward rapidities. All the contributions alongwith feed down ones are displayed separately. Fig. 6 describes the same alongwith the data from CMS detector at 13 TeV for both central and forward rapidities. Our results of CO LDMEs for Υ(2S) have been given in Table 5 along with existing results from different other groups. Our value for $M_L(b\bar{b}([^3S_1]_8 \to \Upsilon(2S))$ is in agreement with the values from other groups also $M_L(b\bar{b}([^1S_0]_8, [^3P_0]_8 \to \Upsilon(2S))$ does not have negative value (which is unphysical) unlike some other groups. The inclusion of 13 TeV data along with the incorporation of feed down from χ_b(3P), is expected to give better constrains of LDMEs.

In [39**?** , 41, 43, 44, 45], authors have considered different combinations of CO LDMEs that has already been described. In Ref. [45], the extracted parameters for Υ(2S) are,

$$M_{0,r_0} = 0.0607 \pm 0.0108 \text{ GeV}^3$$
$$M_{1,r_1} = 0.0108 \pm 0.0020 \text{ GeV}^3$$

with $[3S_1]_1$=4.63 GeV^3 and the values of r_0 and r_1 are same as given before. The χ^2/ndof for the combined fit in our analysis is $\sim$ 2.7.

Having completed Υ(3S) and Υ(2S) parts, we now move on to explore Υ(1S). Alongwith the direct yield, it has feed down contributions from higher S-wave states like Υ(3S) and Υ(2S), as well as P-wave states like χ_b(3P),

Table 6: Comparison of CS elements and CO LDMEs extracted from fitting with experimental data using NRQCD formalism for Υ(1S).

Ref. (LO/NLO)	PDF	m_b (GeV)	$M_L(b\bar{b}([^3S_1]_1 \rightarrow \Upsilon(1S)$ (GeV^3)	$M_L(b\bar{b}([^3S_1]_8 \rightarrow \Upsilon(1S)$ (GeV^3)	$M_L(b\bar{b}([^1S_0]_8, [^3P_0]_8 \rightarrow \Upsilon(1S)$ (GeV^3)	p_T-cut GeV/c
present (LO)	CT18	4.88	10.9	0.0601±0.0017	0.0647±0.0016	8
[39] (LO)	CTEQ4L	4.88	11.1	0.077±0.017	0	2
				0.087±0.016	0	4
				0.106±0.013	0	8
[**?**] (LO)	CTEQ5L	4.77	12.8±1.6	0.116±0.027	0.109±0.062	8
				0.124±0.025	0.111±0.065	
	MRSTLO	4.77	12.8±1.6	0.117±0.030	0.181±0.072	8
				0.130±0.028	0.186±0.075	
[41] (LO)	MSTW08LO	4.88	10.9	0.0477±0.0334	0.0121±0.0400	-
[43] (NLO)	CTEQ6M	4.75	9.282	-0.0041±0.0024	0.0780±0.0043	8
[44] (NLO)	CTEQ6M	PDG	9.282	0.0061±0.0024	0.0895±0.0248	8

χ_b(2P) and χ_b(1P). The associated branching functions are provided in Table 2. The extracted CO-LDMEs for Υ(3S) and Υ(2S) are used for feed down contributions, whereas the LDMEs for the χ_b(nP) states have been taken from Ref. [41, 44] for this present case study. In Fig. 7, we have displayed our NRQCD calculation of production cross-section of Υ(1S) as function of p_T along with the experimental measurements by ATLAS and CMS at $\sqrt{s}$=7 TeV in central rapidities. Finally in Fig. 8, we present our results along with the CMS measurements at 13 TeV with all the components separately to signify their relative contributions.

Table 6 shows our results for Υ(1S) parameters along with the results from different groups. The individual values of LDMEs are in agreement with the values from previous works but with considerable reduction in errors upon inclusion of 13 TeV data sets from CMS. The values of the parameters M_{0,r_0} and M_{1,r_1} extracted in Ref. [45] are,

$$M_{0,r_0} = 0.1370 \pm 0.0111\,\mathrm{GeV}^3,$$
$$M_{1,r_1} = 0.0117 \pm 0.0002\,\mathrm{GeV}^3$$

with $[3S_1]_1$=9.28 GeV^3 keeping r_0 and r_1 same as given before.

Summary. We have presented NRQCD calculations for the differential production cross-sections of Υ states in p+p collisions. Measured transverse momentum distributions of Υ(3S), Υ(2S) and Υ(1S) in p +$\bar{\mathrm{p}}$ collisions at $\sqrt{s}$ = 1.8 TeV and in p+p collisions at 7 TeV and 13 TeV are used to constrain the LDMEs. All the relevant feeddown contributions from higher mass states including the χ_b(3P) are taken in to account. The calculations for Υ(3S), Υ(2S)

and $\Upsilon(1S)$ are compared with the measured data at Tevatron and LHC. The formalism provides very good description of the data in large transverse momentum range at different collision energy. We compare the LDMEs for bottomonia obtained in this analysis with the results from earlier works. At high p_T, the colour singlet contribution is very small and LHC data in large p_T range help to constrain the relative contributions of different colour octet contributions. For Υ states at high p_T, the contribution of the $M_L(b\bar{b}([^3S_1]_8 \rightarrow \Upsilon(nS)))$ is highest which is opposite to the charmonia case where the contribution for the combination of $M_L(c\bar{c}([^1S_0]_8, [^3P_0]_8) \rightarrow \psi)$ is more [54]. In summary, we present a comprehensive lowest-order analysis of hadroproduction data of bottomonia states using the latest parton distribution functions and including very recent LHC data. The feed-down contributions from all the χ_b states are included in the calculations. The values of relevant LDMEs are extracted by doing a simultaneous fit of all the data sets. These values will be useful for predictions of quarkonia cross-section and for the purpose of a comparison with those obtained using the NLO formulations.

3. Bottomonia production mechanism in heavy ion collisions

3.1. Theory overview

3.1.1. Quarkonium in hot medium

Quarkonia production in nuleus-nucleus (A-A) collisions became a vibrant area of research after the seminal paper of Matsui and Satz [4]. It was proposed that quarkonium production would be suppressed compared to the same in the case of p-p collisions. Such a suppression, as proposed, would be a signature of the formation of the QGP phase as the in that phase the strong force would be colour screened. As a result the binding between the heavy quark pairs would be significantly weakened leading to the melting of the corresponding bound states.

However, very soon it was revealed that the picture was not that simple. There are many factors which affect the production of quarkonia in A-A collisions. In fact, quarkonium suppression was also observed in proton-nucleus (pA) collisions, so that part of the nucleus-nucleus suppression is due to cold-nuclear-matter effects. Therefore it is necessary to disentangle hot and cold-medium effects. The CNM effect has mainly two sources : the initial state modification and the final state modification. The initial state modification arises due to modification of parton distribution functions (PDF) inside the nucleus compared to the same inside the protons. The final state modification arises due to the fact the produced quarkonia has to interact with the medium leading to the destabilisation of the bound state. Furthermore, the suppression of quarkonia is thought to be of sequential in nature. The sequential suppression happens as a result of the differences of the binding energy of different bound states. The strongly bound states, such as the $\Upsilon(1S)$ or the J/ψ , melt at higher temperatures. On the other hand more loosely bound staes $\psi(2S)$, χ_c , χ_b , $\Upsilon(2S)$ or $\Upsilon(3S)$ melt at much lower temperatures. This issue throws light towards the estimate of the initial temperature reached in the collisions [61]. However, the prediction of a sequential suppression pattern is complicated feed-down decays of higher-mass resonances and other issues. The production process is further complicated, in the high energy scenario (like LHC), by recombination mechanics. At very high energies abundant production of Q and $\bar{Q}$ may lead to new quarkonia production source. However, this production process is mainly observed in charm quarks and hence in charmonium states. Bottom quarks, being very heavy, do not show any significant recombination effect even in top LHC energies.

To quantify the effect of medium in the quarkonia production scenario one takes recourse to a quantity called the nuclear modification factor (R_{AA}). This quantity is defined as the ratio of the quarkonium yield in the A-A collisions to the same in case of p-p collisions scaled by the number of collisions :

$$R_{AA} = \frac{1}{\langle N_{coll} \rangle} \frac{N_{AA}^{Q\bar{Q}}}{N_{pp}^{Q\bar{Q}}} \tag{9}$$

The ratio will be unity if the physics of the A-A collisions is simply the sum of a large number p-p collisions. The effect of the medium should make it vary from unity.

It has been argued that color screening in a deconfined QCD medium will destroy $Q\overline{Q}$ bound states at sufficiently high temperatures. The binding of heavy quarks depend on the screening radius (r_D). If the binding radius of the heavy quark bound state (r_Q) is is much greater than the screening radius radius then the one heavy quark gets screened from the other and the pair becomes unstable to binding. The screening radius is inversely proportional to the temperature. As the temperature increases the screening radius becomes smaller and smaller compared to the binding radius and the quarkonium states become more and more unstable. Although this idea was proposed long ago, first principle QCD calculations, which go beyond qualitative arguments, have been performed more recently. Such calculations include lattice QCD determinations of quarkonium correlators [62, 63, 64, 65, 66], potential model calculations of the quarkonium spectral functions with potentials based on lattice QCD [61, 67, 68, 69, 70, 71, 72, 73], as well as effective field theory approaches that justify potential models and reveal new medium effects [74, 75, 76, 77]. Furthermore, better modeling of quarkonium production in the medium created by heavy-ion collisions has been achieved. These advancements make it possible to disentangle the cold and hot-medium effects on the quarkonium states, crucial for the interpretation of heavy-ion data.

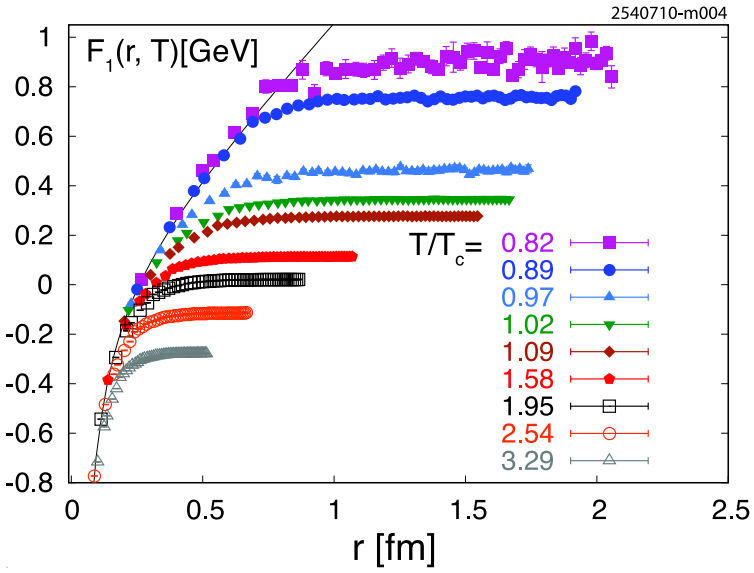

Figure 9: Heavy-quark-singlet free energy versus quark separation calculated in 2+1 flavour QCD on $16^3 \times 4$ lattices at different temperatures [78, 79]

Color screening is studied on the lattice by calculating the spatial correlation function of a static quark and anti-quark in a color-singlet state which propagates in Euclidean time from $\tau = 0$ to $\tau = 1/T$, where T is the temperature.

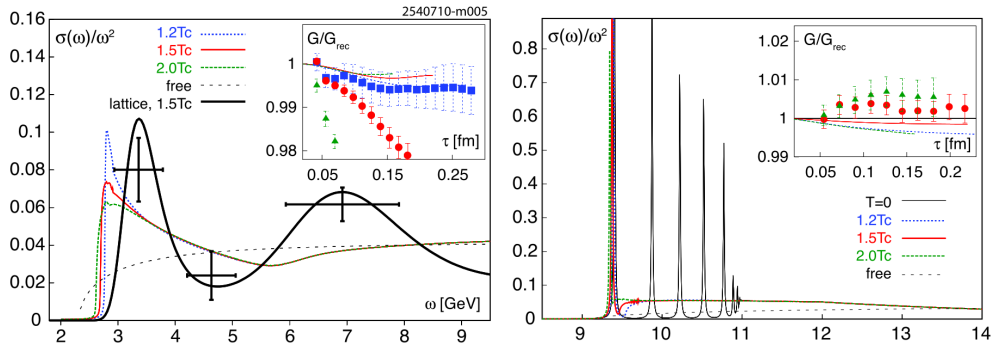

Figure 10: The S-wave charmonium (a) and bottomonium (b) spectral functions calculated in potential models. Insets: correlators compared to lattice data. The *dotted curves* are the free spectral functions.Figure is taken from Ref. [72].

Table 7: Upper bounds on the dissociation temperatures [73].

State	$\chi_{cJ}(1P)$	ψ'	J/ψ	$\Upsilon(2S)$	$\chi_{bJ}(1P)$	$\Upsilon(1S)$
$T_{\rm diss}$	$\leq T_c$	$\leq T_c$	$1.2T_c$	$1.2T_c$	$1.3T_c$	$2T_c$

Lattice calculations of this quantity with dynamical quarks have been reported [80, 78, 79]. The logarithm of the singlet correlation function, also called the singlet free energy, is shown in Fig. 9. As expected, in the zero-temperature limit the singlet free energy coincides with the zero-temperature potential. Figure 9 also illustrates that, at sufficiently short distances, the singlet free energy is temperature independent and equal to the zero-temperature potential. The range of interaction decreases with increasing temperature. For temperatures above the transition temperature, T_c, the heavy-quark interaction range becomes comparable to the charmonium radius. Based on this general observation, one would expect that the charmonium states, as well as the excited bottomonium states, do not remain bound at temperatures just above the deconfinement transition, often referred to as dissociation or melting.

In-medium quarkonium properties are encoded in the corresponding spectral functions, as is quarkonium dissociation at high temperatures. Spectral functions are defined as the imaginary part of the retarded correlation function of quarkonium operators. Bound states appear as peaks in the spectral functions. The peaks broaden and eventually disappear with increasing temperature. The disappearance of a peak signals the melting of the given quarkonium state. The quarkonium spectral functions can be calculated in potential models using the singlet free energy from Fig. 9 or with different lattice-based potentials obtained using the singlet free energy as an input [72, 73]. The results for quenched QCD calculations are shown in Fig. 10 for S-wave charmonium (a) and bottomonium (b) spectral functions [72]. All charmonium states are dissolved in the deconfined phase while the bottomonium 1S state may persist up to $T \sim 2T_c$. An upper bound on the dissociation temperature (the temperatures above which no bound states peaks can be seen in the spectral function and bound state formation is suppressed) can be obtained from the analysis of the spectral functions. Conservative upper limits on the dissociation temperatures for the different quarkonium states obtained from a full QCD calculation [73] are given in Table 7.

Potential model calculations based on lattice QCD, as well as resummed perturbative QCD calculations, indicate

that all charmonium states and the excited bottomonium states dissolve in the deconfined medium. This leads to the reduction of the quarkonium yields in heavy-ion collisions compared to the binary scaling of pp collisions. Recombination and edge effects, however, guarantee a nonzero yield. One of the great opportunities of the LHC heavy-ion program is the ability to study bottomonium yields. From a theoretical perspective, bottomonium is an important and clean probe for at least two reasons. First, the effective field theory approach, which provides a link to first principles QCD, is more applicable for bottomonium due to better separation of scales and higher dissociation temperatures. Second, the heavier bottom quark mass reduces the importance of statistical recombination effects. Experimentally it has less background contribution and is easy to reconstruct. All these properties make bottomonium a good probe of QGP formation in heavy ion collisions.

3.1.2. Cold Nuclear Matter Effects

The baseline for quarkonium production and suppression in heavy-ion collisions should be determined from studies of cold-nuclear-matter (CNM) effects. The name cold matter arises because these effects are observed in hadron-nucleus interactions dense matter effects are much more important compared to the hot matter. There are several CNM effects. The first such effect is the modifications of the parton distribution functions (PDF) in the nucleus compared to that in the nucleon. It depends mainly on two parameters, the momentum fraction of the parton (x) and the scale of the parton-parton interaction (Q^2). The nuclear density modified parton distributed function is known as nPDF. The nPDF to PDF ratio throws light on the modification quarkonia production in the CNM due to the modification of PDFs. This quantity is denoted as $R_i(x, Q^2) = F_i^{p\epsilon A}(x, Q^2)/F_i^p(x, Q^2)$. In the small x regime $(x < 10^{-2})$ this ration is less than unity. This feature is referred to as small-x shadowing. At intermediate x (~ 0.1) the ratio shows a hump like structure a phenomenon known as anti-shadowing. Around $x \approx 0.6$ one observes a dip which is known as EMC effect. The dynamics of partons within the nuclei is affected by the parton saturation which is successfully studied by color glass condensate. In the final state the quarkonia bound state scatter and re-scatter inelastically while passing through the nucleus. This leads the breakup or absorption of the bound state which is estimated by the inelastic cross-section of the quarkonia with the nucleon.

Even though the contributions to CNM effects may seem rather straightforward, there are a number of associated uncertainties. First, while nuclear modifications of the quark densities are relatively well-measured in nuclear deep-inelastic scattering (nDIS), the modifications of the gluon density are not directly measured. The nDIS measurements probe only the quark and antiquark distributions directly. The scaling violations in nDIS can be used to constrain the nuclear gluon density. Overall momentum conservation provides another constraint. However, more direct probes of the gluon density are needed. Current shadowing parametrizations are derived from global fits to the nuclear parton densities and give wide variations in the nuclear gluon density, from almost no effect to very large shadowing at low-x, compensated by strong antishadowing around $x \sim 0.1$.

The nuclear absorption survival probability depends on the quarkonium absorption cross section. There are more inherent uncertainties in absorption than in the shadowing parametrization. It is obtained from data on other processes and is independent of the final state. Typically an absorption cross section is fit to the A dependence of J/ψ and/or $\psi^{'}$ production in pA collision at a given energy. This is rather simplistic since it is unknown whether the object traversing the nucleus is a precursor color-octet state or a fully-formed color-singlet quarkonium state. The J/ψ absorption cross

section at $y \sim 0$ is seen to decrease with energy, regardless of the chosen shadowing parametrization [81].

Recent analyses of J/ψ production in fixed-target interactions [81] show that the effective absorption cross section depends on the energy of the initial beam and the rapidity or x_F of the observed J/ψ . One possible interpretation is that low-momentum color-singlet states can hadronize in the target, resulting in larger effective absorption cross sections at lower center-of-mass energies and backward x_F (or center-of-mass rapidity). At higher energies, the states traverse the target more rapidly so that the x_F values at which they can hadronize in the target move back from midrapidity toward more negative x_F. Finally, at sufficiently high energies, the quarkonium states pass through the target before hadronizing, resulting in negligible absorption effects. Thus the *effective* absorption cross section decreases with increasing center-of-mass energy because faster states are less likely to hadronize inside the target.

This is a very simplistic picture. In practice, cold-nuclear-matter effects (initial-state energy loss, shadowing, final-state breakup, *etc.*) depend differently on the quarkonium kinematic variables and the collision energy. It is clearly unsatisfactory to combine all these mechanisms into an *effective* absorption cross section, as employed in the Glauber formalism, that only evaluates final-state absorption. Simply taking the $\sigma_{\rm abs}$ obtained from the analysis of the pA data and using it to define the Pb+Pb baseline is not be sufficient. A better understanding of absorption requires more detailed knowledge of the production mechanisms which it self are largely unknown.

3.1.3. Collisional dissociation of quarkonia from final-state interactions

Modification of quarkonia in the presence of QGP. In the kinetic approach [82], the proper time τ evolution of the quarkonia population N_Q is given by the rate equation

$$\frac{dN_Q}{d\tau} = -\lambda_D \rho_g N_Q + \lambda_F \frac{N_{q\bar{q}}^2}{V(\tau)}, \tag{10}$$

where $V(\tau)$ is the volume of the deconfined spatial region and $N_{q\bar{q}}$ is the number of initial heavy quark pairs produced per event depending on the centrality defined by the number of participants $N_{\rm part}$. The λ_D is the dissociation rate obtained by the dissociation cross section averaged over the momentum distribution of gluons and λ_F is the formation rate obtained by the formation cross section averaged over the momentum distribution of heavy quark pair q and $\bar{q}$. ρ_g is the density of thermal gluons. The number of quarkonia at freeze-out time τ_f is given by the solution of Eq. (10),

$$N_Q(p_T) = S(p_T)\, N_Q^{\rm PbPb}(p_T) + N_Q^F(p_T). \tag{11}$$

Here $N_Q^{\rm PbPb}(p_T)$ is the number of initially-produced quarkonia (including shadowing) as a function of p_T and $S(p_T)$ is their survival probability from gluon collisions at freeze-out,

$$S(p_T) = \exp\left(- \int_{\tau_0}^{\tau_f} f(\tau) \lambda_{\rm D}(T, p_T)\, \rho_g(T)\, d\tau \right). \tag{12}$$

The temperature $T(\tau)$ and the QGP fraction $f(\tau)$ evolve from initial time τ_0 to freeze-out time τ_f due to expansion of the QGP. The initial temperature and the evolution is dependent on collision centrality $N_{\rm part}$. $N_Q^F(p_T)$ is the number of regenerated quarkonia per event,

$$N_Q^F(p_T) = S(p_T) N_{q\bar{q}}^2 \int_{\tau_0}^{\tau_f} \frac{\lambda_{\rm F}(T, p_T)}{V(\tau)\, S(\tau, p_T)} d\tau. \tag{13}$$

The nuclear modification factor (R_{AA}) can be written as

$$R_{AA}(p_T) = S(p_T)\, R(p_T) + \frac{N_Q^F(p_T)}{N_Q^{pp}(p_T)}. \tag{14}$$

Here $R(p_T)$ is the shadowing factor. R_{AA} as a function of collision centrality, including regeneration, is

$$R_{AA}(N_{\rm part}) = \frac{\int_{p_T\,\rm cut} N_Q^{pp}(p_T) S(p_T)\, R(p_T) dp_T}{\int_{p_T\,\rm cut} N_Q^{pp}(p_T) dp_T} + \frac{\int_{p_T\,\rm cut} N_Q^{F}(p_T) dp_T}{\int_{p_T\,\rm cut} N_Q^{pp}(p_T) dp_T} \tag{15}$$

Here $p_{T\ \rm cut}$ defines the p_T range for a given experimental acceptance. $N_Q^{pp}(p_T)$ is the unmodified p_T distribution of quarkonia obtained by NLO calculations and scaled to a particular centrality of the Pb+Pb collisions.

The evolution of the system for each centrality bin is governed by an isentropic cylindrical expansion with volume element

$$V(\tau) = \tau\, \pi\, (R + \frac{1}{2} a_T\, \tau^2)^2, \tag{16}$$

where $a_T = 0.1\, c^2$ fm^{-1} is the transverse acceleration [83]. The initial transverse size, R, as a function of centrality is

$$R(N_{\rm part}) = R_{0-5\%} \sqrt{\frac{N_{\rm part}}{(N_{\rm part})_{0-5\%}}}, \tag{17}$$

where $R_{0-5\%} = 0.96\, R_{\rm Pb}$ and $R_{\rm Pb}$ is the radius of the lead nucleus. The evolution of entropy density for each centrality is obtained by entropy conservation, $s(T)\, V(\tau) = s(T_0)\, V(\tau_0)$. The equation of state (EOS) obtained from Lattice QCD, along with a hadronic resonance gas, [84] is used to obtain the temperature as a function of proper time τ. The initial entropy density for each centrality is calculated using

$$s(\tau_0) = s(\tau_0)|_{0-5\%} \left(\frac{dN/d\eta}{N_{\rm part}/2}\right) \left(\frac{dN/d\eta}{N_{\rm part}/2}\right)^{-1}_{0-5\%}. \tag{18}$$

Measured values of $(dN/d\eta)/(N_{\rm part}/2)$ as a function of $N_{\rm part}$ [85, 86] are used in the calculations. The initial entropy density, $s(\tau_0)|_{0-5\%}$, for 0-5% centrality is

$$s(\tau_0)|_{0-5\%} = \frac{a_m}{V(\tau_0)|_{0-5\%}} \left(\frac{dN}{d\eta}\right)_{0-5\%}. \tag{19}$$

Here a_m (= 5) is a constant which relates the total entropy to the total multiplicity $dN/d\eta$. It is obtained from hydrodynamic calculations [87]. We estimate the initial temperature, T_0, in the 0-5% most central collisions from the total multiplictity in the rapidity region of interest, assuming that the initial time is $\tau_0 = 0.3$ fm/c over all rapidity. The total multiplicity in a given rapidity region is 3/2 times the charged particle multiplicity in Pb+Pb collisions at 2.76 TeV. With the lattice EOS, at midrapidity, with $(dN_{\rm ch}/d\eta)_{0-5\%} = 1600$ [85, 86], we find $T_0 = 0.484$ GeV. Likewise, at forward rapiidity, $2.5 \le y \le 4$ [88], $T_0 = 0.427$ GeV. The (proper) time evolution of temperature is shown in Fig. 11(a) and that of QGP fraction in Fig. 11(b), in the case of the most central (0-5%) collisions. Here we compare the evolution obtained with longitudinal and cylindrical expansions using both a first order and the lattice EOS. For the first order EOS, T_c = 0.170 GeV. The QGP fraction goes from 1 to 0 at T_c assuming a mixed phase of QGP and hadrons. The QGP fraction in case of lattice EOS governs the number of degrees of freedom, decided by the entropy density. It is fixed to unity above an entropy density corresponding to a 2-flavour QGP and fixed to zero below entropy density for a hot resonance gas. The freeze out temperature in all cases is $T_f = 0.140$ GeV.

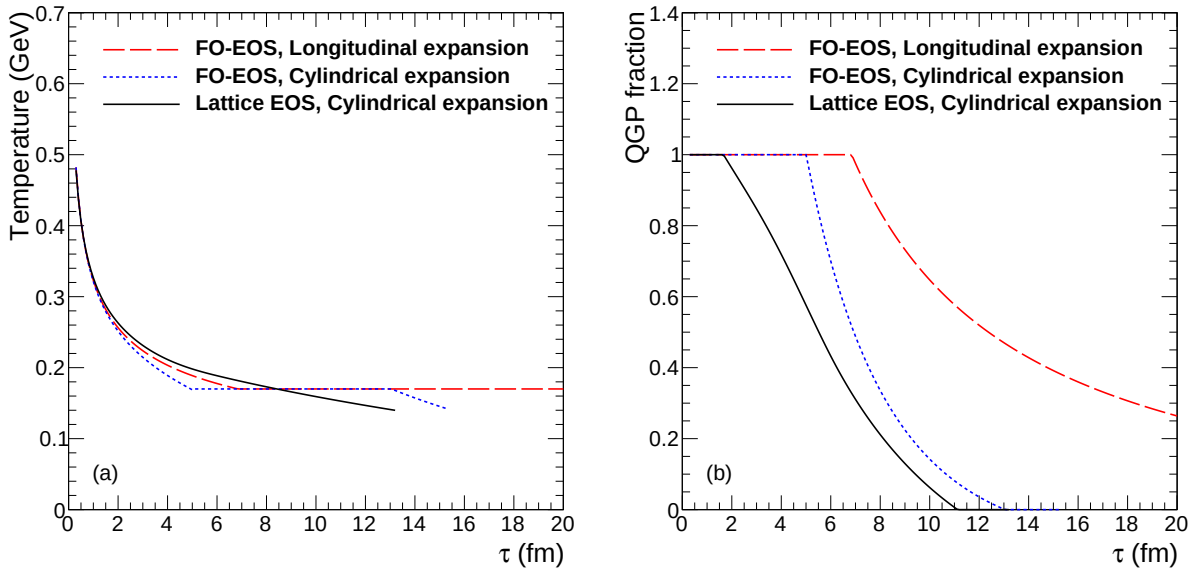

Figure 11: (Color online) (a) Temperature and (b) QGP fraction in the system as a function of proper time τ in case of the most central (0-5%) collisions for longitudinal and cylindrical expansions using first order and lattice equation of state.

3.2. Dissociation Rate

In the color dipole approximation, the gluon dissociation cross section as function of gluon energy, q^0, in the quarkonium rest frame is [89]

$$\sigma_D(q^0) = \frac{8\pi}{3}\,\frac{16^2}{3^2}\,\frac{a_0}{m_q}\,\frac{(q^0/\epsilon_0 - 1)^{3/2}}{(q^0/\epsilon_0)^5}, \tag{20}$$

where ϵ_0 is the quarkonia binding energy and m_q is the charm/bottom quark mass and $a_0 = 1/\sqrt{m_q\epsilon_0}$. The values of ϵ_0 are taken as 0.64 and 1.10 GeV for the ground states, J/ψ and Υ(1S), respectively [90]. For the first excited state of bottomonia, Υ(2S), we use dissociation cross section from Ref. [91].

Figure 12 shows the gluon dissociation cross sections of J/ψ and Υ(1S) as a function of gluon energy. The dissociation cross section is zero when the gluon energy is less than the binding energy of the quarkonia. It increases with gluon energy and reaches a maximum at 1.2 (1.5) GeV for J/ψ ($\Upsilon(1S)$). At higher gluon energies, the interaction probability decreases. The gluon energy q^0 is related to the square of the center of mass energy s, of the quarkonium-gluon system by

$$q^0 = \frac{s - M_Q^2}{2\,M_Q} \tag{21}$$

where $s = M_Q^2 + 2p_g\sqrt{M_Q^2 + p^2} - 2p_g\,p\cos\theta$, and M_Q and p are mass and momentum of quarkonium and θ is angle between the quarkonium and the gluon. We calculate the dissociation rate as a function of quarkonium momentum by integrating the dissociation cross section over thermal gluon momentum distribution $f_g(p_g)$,

$$\begin{aligned}\lambda_D\rho_g &= \langle\sigma v_{\rm rel}\rangle\,\rho_g = \frac{g_g}{(2\pi)^3}\int d^3p_g\, f_g(p_g)\,\sigma_D(s)v_{\rm rel}(s) \\ &= \frac{g_g}{(2\pi)^3}\int dp_g 2\pi p_g^2 f_g(p_g)\int d\cos\theta\,\sigma_D(s)\,v_{\rm rel}(s),\end{aligned} \tag{22}$$

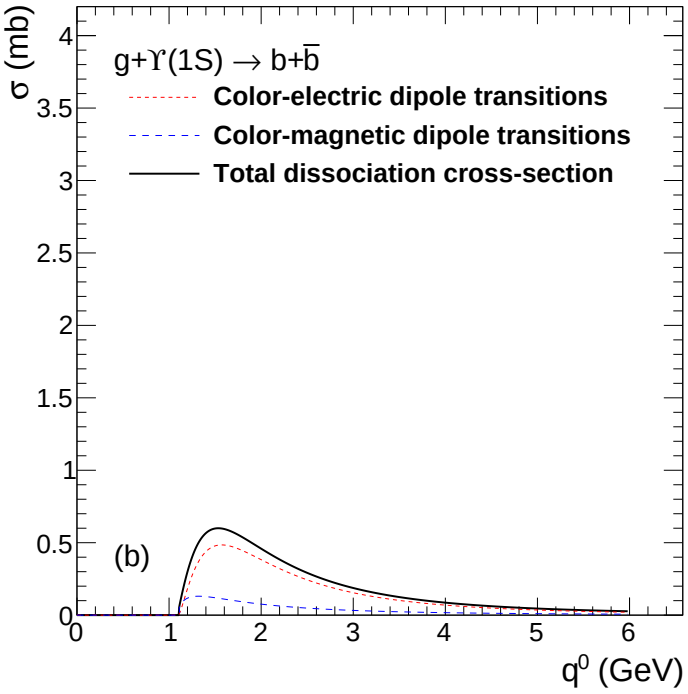

Figure 12: (Color online) Gluon dissociation cross section of quarkonia as a function of gluon energy (q^0) in quarkonia rest frame.

where $\sigma_D(s) = \sigma_D(q^0(s))$. The relative velocity, $v_{\rm rel}$, between the quarkonium and the gluon is

$$v_{\rm rel} = \frac{s - M_Q^2}{2p_g\sqrt{M_Q^2 + p^2}}. \tag{23}$$

The J/ψ gluon dissociation rates as a function of T are shown in Fig. 13(a) and as a function of p_T in Fig. 13(b). The dissociation rate increases with temperature due to the increase in gluon density. The dissociation rate is maximum when the quarkonium is at rest and decreases with p_T.

3.3. Formation Rate

We can calculate the formation cross section from the dissociation cross section using detailed balance [82, 92],

$$\sigma_F = \frac{48}{36}\,\sigma_D(q^0)\frac{(s - M_Q^2)^2}{s(s - 4m_q^2)}. \tag{24}$$

The formation rate of quarkonium with momentum $\mathbf{p}$ can be written as

$$\frac{d\lambda_F}{d\mathbf{p}} = \int d^3p_1\, d^3p_2\, \sigma_F(s)\, v_{\rm rel}(s)\, f_q(p_1)\, f_{\bar{q}}(p_2)\, \delta(\mathbf{p} - (\mathbf{p_1} + \mathbf{p_2})). \tag{25}$$

Here $f_{q/\bar{q}}(p)$ are taken as thermal distribution function of $q/\bar{q}$ which are normalized to one, $\int f_q(p)d^3p = 1$ and $v_{\rm rel}$ is relative velocity of the $q\bar{q}$ quark pair,

$$v_{\rm rel} \;=\; \frac{\sqrt{(p_1.p_2)^2 - m_q^4}}{E_1\,E_2}. \tag{26}$$

Here $p_1 = (E_1, \mathbf{p_1})$ and $p_2 = (E_2, \mathbf{p_2})$ are the four momenta of the heavy quark and antiquark respectively. Figure 14 (a) shows the variation of the formation rate as a function of T and Fig. 14 (b) shows as a function of J/ψ p_T. The

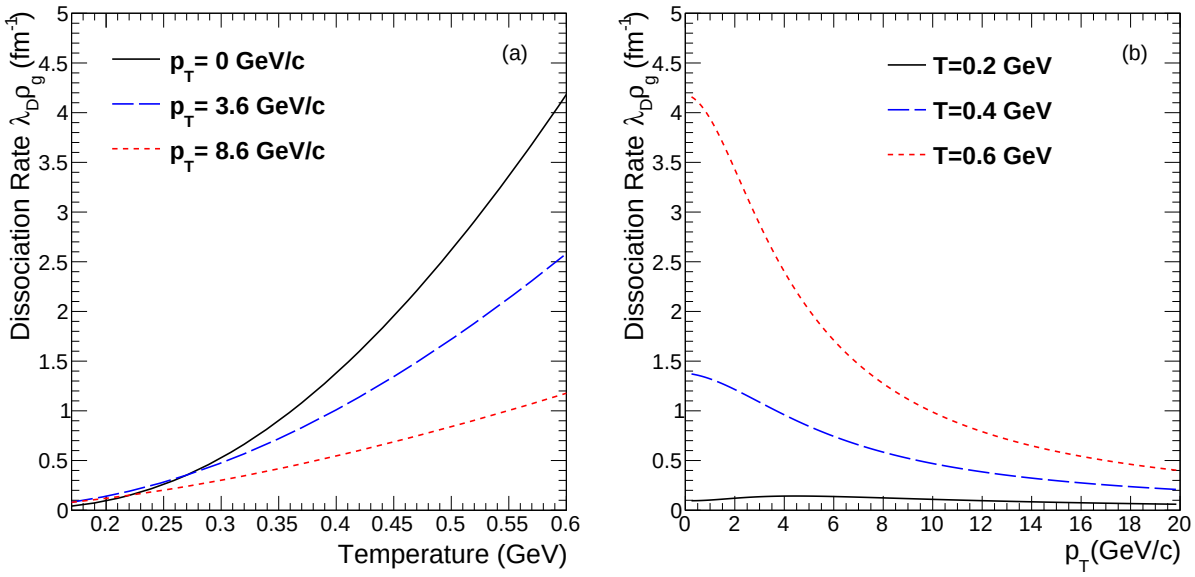

Figure 13: (Color online) Gluon dissociation rate of J/ψ as a function of (a) temperature and (b) transverse momentum.

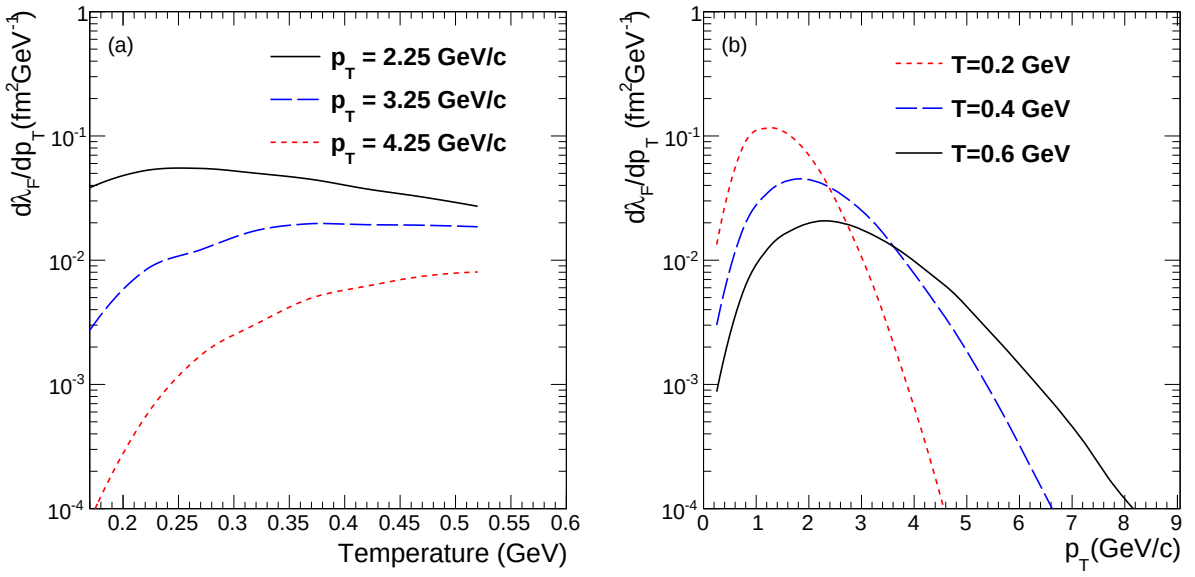

Figure 14: (Color online) Formation rate of J/ψ as a function of (a) temperature and (b) transverse momentum.

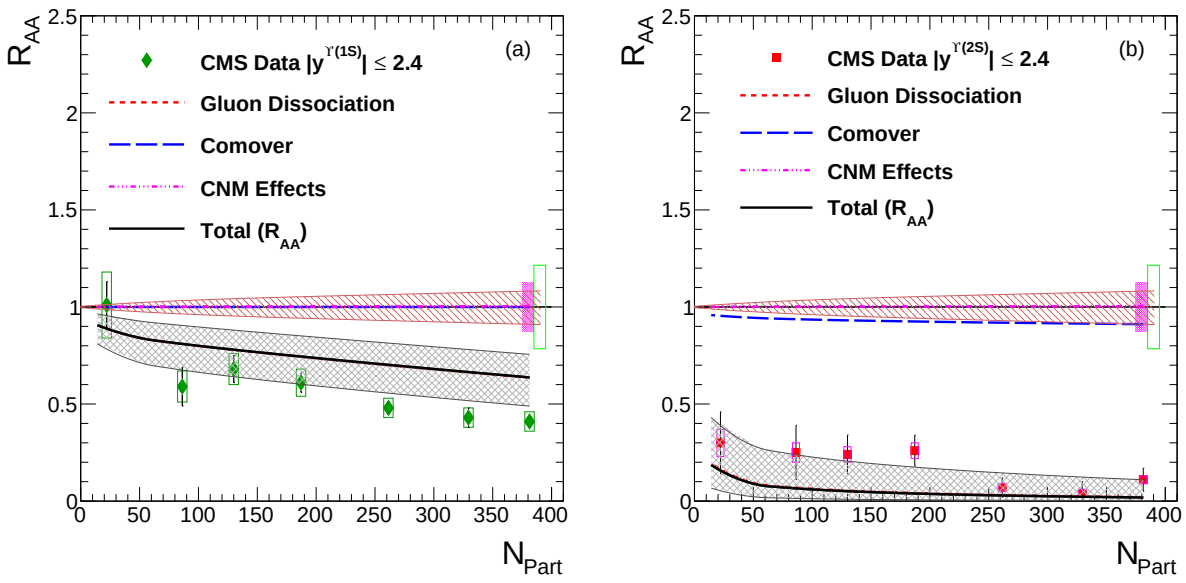

Figure 15: (Color online) Calculated nuclear modification factor (R_{AA}) compared with CMS (a) Υ(1S) and (b) Υ(2S) measurements. Regeneration is assumed to be negligible.

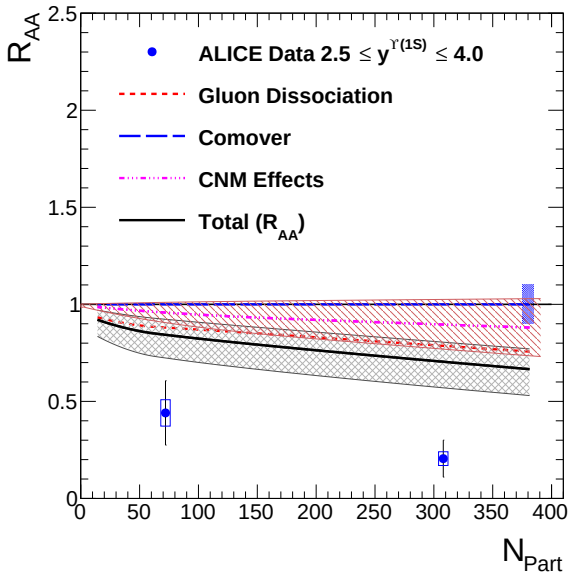

Figure 16: (Color online) Calculated nuclear modification factor (R_{AA}) compared with ALICE Υ(1S) measurement in forward rapidity.

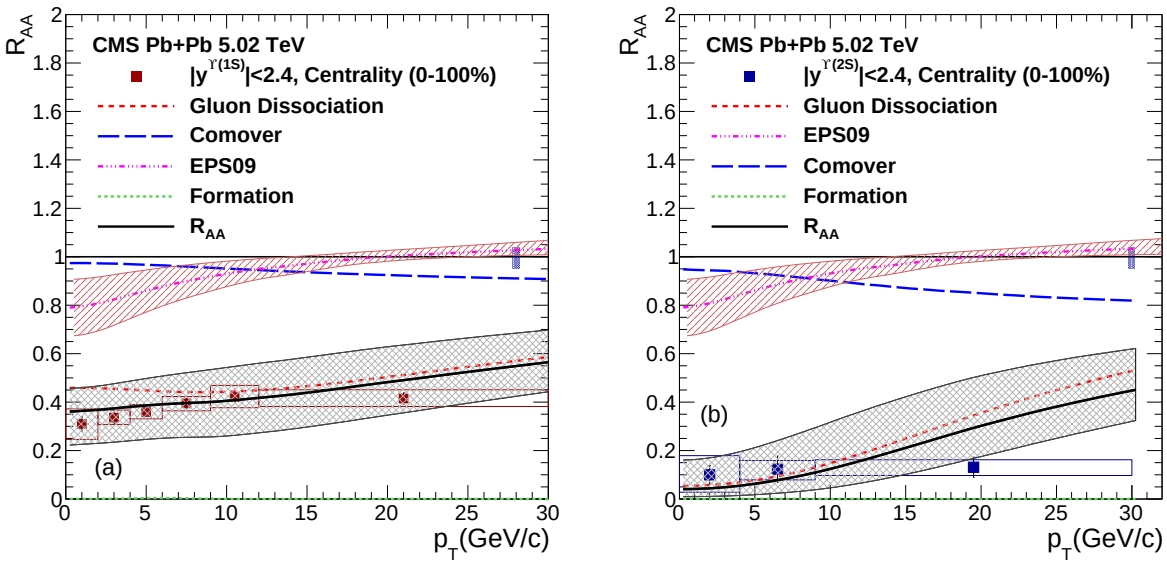

Figure 17: (Color online) Calculated nuclear modification factor (R_{AA}) of (a) Υ(1S) and (b) Υ(2S) as a function of p_T compared with CMS measurements [30]. The global uncertainty in R_{AA} is shown as a band around the line at 1.

J/ψ generated from recombination of uncorrelated heavy quark pairs will have softer p_T distributions than those of J/ψ's coming from the initial hard scatterings. Thus the effect of recombination will be important only at low p_T.

Figure 15 (a) demonstrates the contributions from different processes to the centrality dependence of the Υ(1S) nuclear modification factor, along with the midrapidity data from CMS [93]. The calculations underestimate the suppression but reproduce the shape of centrality dependence. This may be due to the feed down effects from the excited states. Figure 15 (b) shows the same for the Υ(2S) nuclear modification factor along with the CMS measurements at midrapidity. The excited Υ(2S) states are highly suppressed. The effect of regeneration, not shown, is negligible for the Υ states. Figure 16 shows the forward rapidity ALICE measurement of the Υ(1S) nuclear modification factor [94] along with our calculations. The suppression due to thermal gluon dissociation is smaller than the measured suppression which may be due to the effect of feed down from the Υ(2S) and higher states. However the measurement is consistent with the suppression of Υ(2S) and Υ(3S) contribution, along with suppression of the Υ(1S) by gluon dissociation.

Figure 17(a) and (b) show the calculations of contributions to the nuclear modification factor, R_{AA}, for the Υ(1S) and Υ(2S) respectively as a function of p_T compared with the mid rapidity measurements from CMS [30]. The gluon dissociation mechanism combined with the pion dissociation and shadowing corrections gives good description of data in mid p_T range ($p_T \approx$ 5-10 GeV/c) for both Υ(1S) and Υ(2S). The contribution from the regenerated Υs is negligible even at LHC energies. Our calculations under-predict the suppression observed at the highest measured p_T for Υ(1S) and Υ(2S) which is similar for the case of J/ψ. The states Υ(1S) and Υ(2S) also have feed-down contributions from decays of higher $b\bar{b}$ bound states. The nuclear modification factor, R_{AA} is obtained taking into account the feed-down corrections as follows

$$R_{AA}^{\Upsilon(3S)} = R_{AA}^{\Upsilon(3S)} \tag{27}$$

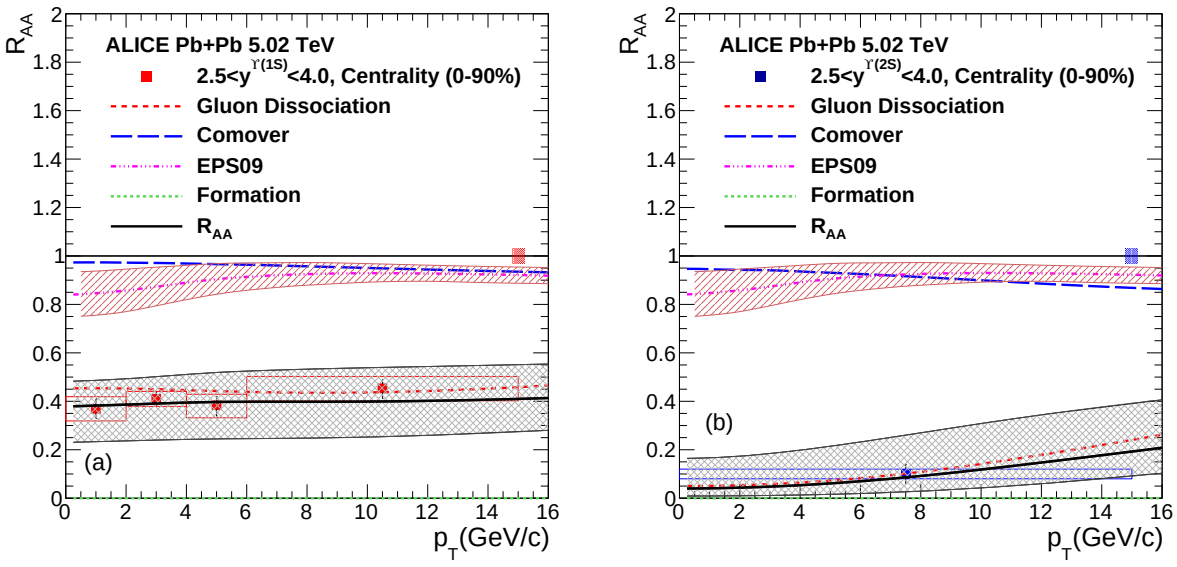

Figure 18: (Color online) Calculated nuclear modification factor (R_{AA}) of (a) Υ(1S) and (b) Υ(2S) as a function of p_T in the kinematic range of ALICE detector at LHC [**?**]. The global uncertainty in R_{AA} is shown as a band around the line at 1.

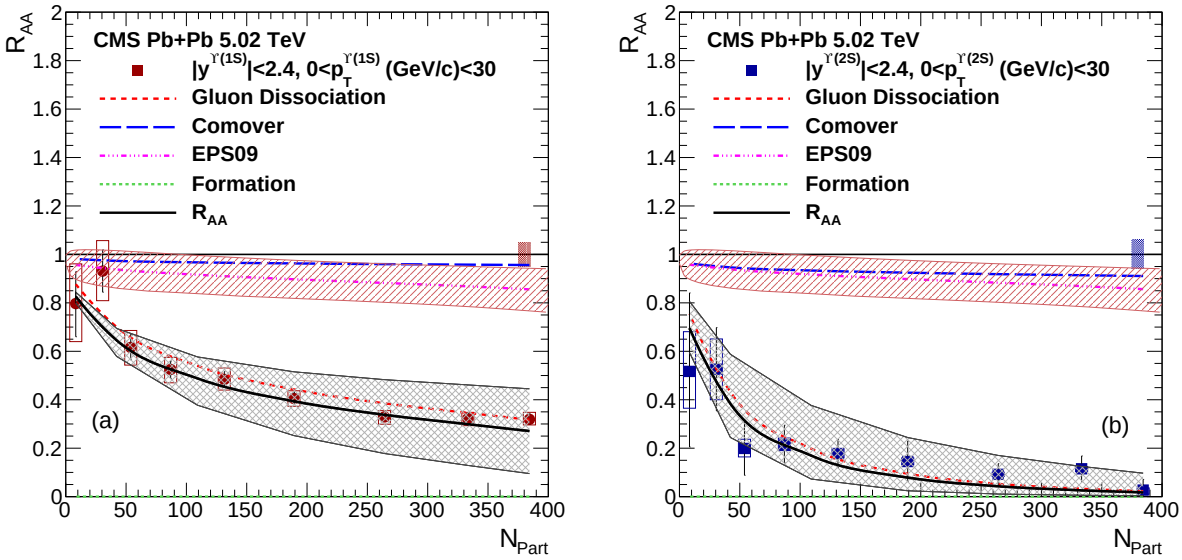

Figure 19: (Color online) Calculated nuclear modification factor (R_{AA}) of (a) Υ(1S) and (b) Υ(2S) as a function of centrality of the collisions compared with the CMS measurements [30].The global uncertainty in R_{AA} is shown as a band around the line at 1.

$$R_{AA}^{\Upsilon(2S)} = f_1 R_{AA}^{\Upsilon(2S)} + f_2 R_{AA}^{\Upsilon(3S)} \tag{28}$$

$$R_{AA}^{\Upsilon(1S)} = g_1 R_{AA}^{\Upsilon(1S)} + g_2 R_{AA}^{\chi_b(1P)} + g_3 R_{AA}^{\Upsilon(2S)} + g_4 R_{AA}^{\Upsilon(3S)} \tag{29}$$

The factors f's and g's are obtained from CDF measurement [95]. The values of g_1, g_2, g_3 and g_4 are 0.509, 0.27, 0.107 and 0.113 respectively. Here g_4 is assumed to be the combined fraction of Υ(3S) and χ_b(2P). The values of f_1 and f_2 are taken as 0.50 [96].

Figure 18(a) and (b) show the model prediction of the nuclear modification factor, R_{AA}, for the Υ(1S) and Υ(2S) respectively as a function of p_T in the kinematic range covered by ALICE detector. The ALICE data [**?**] is well described by our model.

Figure 19(a) depicts the calculated centrality dependence of the Υ(1S) nuclear modification factor, along with the midrapidity data from CMS [30]. Our calculations combined with the pion dissociation and shadowing corrections gives very good description of the measured data. Figure 19(b) shows the same for the Υ(2S) along with the midrapidity CMS measurements. The suppression of the excited Υ(2S) states is also well described by our model. As stated earlier, the effect of regeneration is negligible for Υ states.

Figure **??**(a) shows the forward rapidity ALICE measurement of the Υ(1S) nuclear modification factor [**?**] along with our calculations. The suppression due to thermal gluon dissociation describes the measured data after including the comover and shadowing corrections. Figure **??**(b) shows the calculations for the Υ(2S) nuclear modification factor in ALICE detector kinematic range. The suppression due to thermal gluon dissociation describes the ALICE measurements after including the comover and shadowing corrections.

3.3.1. Suppression in anisotropic medium

In a series of papers people have studied bottomonia suppression using anisotropic hydrodynamics. There are two major *new* ingredients to this work : (1) the first-principles calculation of the thermal widths of heavy quarkonium states and (2) consideration of the momentum anisotropy of the plasma.

In these works the phase-space distribution of gluons in the local rest frame is assumed to be

$$f(\mathbf{x}, \mathbf{p}) = f_{\rm iso}\left(\sqrt{\mathbf{p}^2 + \xi(\mathbf{p}\cdot\mathbf{n})^2}/p_{\rm hard}\right) \tag{30}$$

In the above equation ξ is a measure of the degree of anisotropy of the plasma.

$$\xi = \frac{1}{2}\langle \mathbf{p}_\perp^2 \rangle / \langle p_z^2 \rangle - 1 \tag{31}$$

where p_z and $\mathbf{p}_\perp$ are the partonic longitudinal and transverse momenta in the local rest frame, respectively. In equation 30, $p_{\rm hard}$ is the momentum scale of the particles and can be identified with the temperature in an isotropic plasma.

An approximate form of the real perturbative heavy quark potential as function of ξ can be written as [97] (for

$N_c = 3$ and $N_f = 2$).

$$\begin{aligned} Re[V_{\rm pert}] &= -\alpha \exp(-\mu r)/r \\ \left(\frac{\mu}{m_D}\right)^{-4} &= 1 + \xi\left(1 + \frac{\sqrt{2}(1+\xi)^2\left(\cos(2\theta)-1\right)}{(2+\xi)^{5/2}}\right) \end{aligned} \tag{32}$$

where $\alpha = 4\alpha_s/3$, $m_D^2 = (1.4)^2 16\pi\alpha_s\, p_{\rm hard}^2/3$ is the isotropic Debye mass and θ is the angle with respect to the beamline. The factor of $(1.4)^2$ accounts for higher-order corrections to the isotropic Debye mass [98].

This perturbative potential, given in equation (30) is modified to include the non-perturbative (long range) contributions. The modified real part of the potential is given as [97]

$$\begin{aligned} Re[V] &= -\frac{\alpha}{r}\left(1+\mu\, r\right)\exp\left(-\mu\, r\right) + \frac{2\sigma}{\mu}\left[1-\exp\left(-\mu\, r\right)\right] \\ &\quad -\sigma\, r\, \exp(-\mu\, r) - \frac{0.8\,\sigma}{m_Q^2\, r}\,, \end{aligned} \tag{33}$$

where the last term is a temperature- and spin-independent quark mass correction [99] and $\sigma = 0.223$ GeV is the string tension. Here α is chosen to be 0.385 to match zero temperature binding energy data for heavy quark states [97]. The imaginary part of the potential is taken as the same as the perturbative heavy quark potential up to linear order in ξ

$$Im[V_{\rm pert}] = -\alpha p_{\rm hard}\Big\{\phi(\hat{r}) - \xi\left[\psi_1(\hat{r},\theta) + \psi_2(\hat{r},\theta)\right]\Big\}, \tag{34}$$

where $\hat{r} = m_D r$ and ϕ, ψ_1, and ψ_2 are defined as

$$\phi(\hat{r}) = 2\int_0^\infty dz \frac{z}{(z^2+1)^2}\left[1 - \frac{\sin\left(z\hat{r}\right)}{\hat{r}}\right], \tag{35}$$

$$\psi_1(\hat{r},\theta) = \int_0^\infty dz \frac{z}{(z^2+1)^2}\left(1 - \frac{3}{2}\left[\sin^2\theta \frac{\sin(z\,\hat{r})}{z\,\hat{r}} + (1-3\cos^2\theta)G(\hat{r},z)\right]\right), \tag{36}$$

$$\psi_2(\hat{r},\theta) = -\int_0^\infty dz \frac{\frac{4}{3}z}{(z^2+1)^3}\left(1 - 3\left[\left(\frac{2}{3} - \cos^2\theta\right)\frac{\sin(z\,\hat{r})}{z\,\hat{r}} + (1-3\cos^2\theta)G(\hat{r},z)\right]\right). \tag{37}$$

where $G(\hat{r},z)$ is the Meijer G-function. The full model potential, given by $V = Re[V] + iIm[V]$, is used to solve the Schrödinger equation.

Solution of the Schrödinger equation gives the real and imaginary parts of the binding energy of the states. The imaginary part defines the instantaneous width of the state $Im[E_{\rm bind}(p_{\rm hard},\xi)] \equiv -\Gamma_T(p_{\rm hard},\xi)/2$. The resulting width $\Gamma_T(\tau)$ implicitly depends on the initial temperature of the system.

The following rate equation is used to account for in-medium bottomonia state decay,

$$\frac{dn(\tau,\mathbf{x}_\perp,\varsigma)}{d\tau} = -\Gamma(\tau,\mathbf{x}_\perp,\varsigma)n(\tau,\mathbf{x}_\perp,\varsigma), \tag{38}$$

where $\tau = \sqrt{t^2-z^2}$ is the longitudinal proper time, $\mathbf{x}_\perp$ is the the transverse coordinate and $\varsigma = \text{arctanh}(z/t)$ is the the spatial rapidity. The rate of decay is computed by [96]

$$\Gamma(\tau,\mathbf{x}_\perp,\varsigma) = 2Im[E_{\rm bind}(\tau,\mathbf{x}_\perp,\varsigma)] \qquad Re[E_{\rm bind}(\tau,\mathbf{x}_\perp,\varsigma)] > 0 \tag{39}$$

$$= \gamma_{\rm dis} \qquad Re[E_{\rm bind}(\tau,\mathbf{x}_\perp,\varsigma)] \leq 0. \tag{40}$$

In order to look at the suppression one has to calculate R_{AA}. The algorithm to obtain R_{AA} is the following. First one obtains

$$\bar{\gamma}(\mathbf{x}_\perp, p_T, \varsigma, b) \equiv \Theta(\tau_f - \tau_{\rm form}(p_T)) \int_{\max(\tau_{\rm form}(p_T),\tau_0)}^{\tau_f} d\tau\, \Gamma_T(\tau, \mathbf{x}_\perp, \varsigma, b) \tag{41}$$

where ς is the spatial rapidity. From this one obtains

$$R_{AA}(\mathbf{x}_\perp, p_T, \varsigma, b) = \exp(-\bar{\gamma}(\mathbf{x}_\perp, p_T, \varsigma, b)) \tag{42}$$

Finally, one averages over $\mathbf{x}_\perp$ to obtain

$$\langle R_{AA}(p_T, \varsigma, b)\rangle \equiv [\int_{\mathbf{x}_\perp} d\mathbf{x}_\perp\, T_{AA}(\mathbf{x}_\perp)\, R_{AA}(\mathbf{x}_\perp, p_T, \varsigma, b)]/[\int_{\mathbf{x}_\perp} d\mathbf{x}_\perp\, T_{AA}(\mathbf{x}_\perp)] \tag{43}$$

3.3.2. Statistical (re) generation models

We can include the regenration part from our calculations. These effects are also small.

3.3.3. Comover models

The suppression of quarkonia by comoving pions can be calculated by folding the quarkonium-pion dissociation cross section $\sigma_{\pi Q}$ over thermal pion distributions [100]. It is expected that at LHC energies, the comover cross section will be small [81]. The pion-quarkonia cross section is calculated by convoluting the gluon-quarkonia cross section σ_D over the gluon distribution inside the pion [91],

$$\sigma_{\pi Q}(p_\pi) = \frac{p_+^2}{2(p_\pi^2 - m_\pi^2)} \int_0^1 dx\, G(x)\, \sigma_D(x p_+/\sqrt{2}), \tag{44}$$

where $p_+ = (p_\pi + \sqrt{p_\pi^2 - m_\pi^2})/\sqrt{2}$. The gluon distribution, $G(x)$, inside a pion is given by the GRV parameterization [101]. The pion momentum p_π is related to center of mass energy $\sqrt{s}$ of pion-J/ψ system by $p_\pi = (s - M_Q^2 - m_\pi^2)/(2M_Q)$. The dissociation rate λ_{D_π} can be written as

$$\begin{aligned} \lambda_{D_\pi}\, \rho_\pi &= \frac{g_\pi}{(2\pi)^3} \int d^3p_\pi\, f_\pi(p) \sigma_{\pi Q}(s) v_{\rm rel}(s) \\ &= \frac{g_\pi}{(2\pi)^3} \int dp_\pi\, 2\pi p_\pi^2 f_\pi(p_\pi) \int d\cos\theta\, \sigma_{\pi Q}(s)\, v_{\rm rel}(s) \Theta(s - 4m_D^2), \end{aligned} \tag{45}$$

where $f_\pi(p_\pi, T)$ is the thermal pion distribution. The pion density ρ_π is

$$\rho_\pi = \frac{g_\pi}{(2\pi)^3} \int d^3p_\pi\, f_\pi(p_\pi). \tag{46}$$

The survival probability from pion collisions at freeze-out time τ_f is written as

$$S_\pi(p_T) = \exp\left(-\int_{\tau_0}^{\tau_f} d\tau\, (1 - f(\tau)) \lambda_{D_\pi}(T, p_T)\, \rho_\pi(T)\right). \tag{47}$$

The hadronic fraction (1-$f(\tau)$) is zero in QGP phase. The probability $S_\pi(p_T)$ multiplies $S(p_T)$ in Eq. (14).

3.3.4. Summary of theoretical models for experimental comparison

We will write the summary for all different type of quarkonia model here.

3.4. Experimental overview of Bottomonia results at RHIC and LHC

The primary motivation for studying high-energy heavy ion collisions is to better understand the hot and dense matter produced in these interactions. Lattice quantum chromodynamics (LQCD) calculations indicate that at sufficiently high temperatures a crossover occurs from hadronic matter to a strongly interacting system of deconfined quarks and gluons known as "quark-gluon plasma" (QGP). One of the most prominent signatures of QGP formation is that the production of quarkonia, the bound states of a heavy quark and its antiquark, is suppressed with respect to expectations from scaling the yields in proton-proton collisions by the number of binary nucleon-nucleon (NN) collisions. This suppression arises because the quarkonia binding is weakened by color screening caused by the surrounding partons in the medium [4]. Therefore the extent of the quarkonia suppression is expected to be sequentially ordered by the binding energies of the quarkonia states. Because of the binding energy dependence of the screening, the bottomonium states (Υ(1S), Υ(2S), Υ(3S), χ_b, etc.) are particularly useful probes to understand the space-time evolution of the QGP. The sequential suppression of the yield of Υ(nS) states was first observed by CMS at $\sqrt{s_{NN}}$ =2.76 TeV [102, 93]. More recently, results with improved statistical precision have been reported by both the ALICE and CMS Collaborations at $\sqrt{s_{NN}}$ =5.02 TeV [103, 30, 104]. The suppression of the Υ(1S) meson has also been studied at $\sqrt{s_{NN}}$ =200 GeV at RHIC [105].

The screening due to the QGP can also result in an azimuthal asymmetry in the observed yields of quarkonia. In non-central heavy ion collisions, the produced QGP has a lenticular shape in the transverse plane. Consequently, the average path length for quarkonia traveling through the medium depends on the direction taken with respect to this shape, with a larger suppression in the direction of the longer axis [106]. The anisotropic distribution of particles can be characterized by the magnitudes of the Fourier co-efficients (v_n) of the azimuthal correlation of particles [107]. By studying the azimuthal distribution of the quarkonia, it is possible to develop a more comprehensive understanding of the dynamics of their production. The available experimental data, spanning from 0.20 to 5.02 TeV, have provided new insight into the thermal properties of the QGP. In this section we review the current status of the experimental measurement of R_{AA} and v_2 for Υ states. The data from different experiments are comapred and physics insights from them is discussed.

3.4.1. Υ(nS) R_{AA} at the LHC

Measurement by CMS, ATLAS and ALICE. The bottomonia states (Υ(nS)) are measured at the LHC with very good statistical precision [93, 94, 102, 108]. The CMS measurements at $\sqrt{s_{NN}}$ =2.76 TeV [93, 102] reveal a clear proof of sequential suppression : Υ(2S) and Υ(3S) are more suppressed relative to the ground state Υ(1S). The individual Υ states are also found to be suppressed in the PbPb collisions relative to the production in the pp collisions. The Υ nuclear modification factor, R_{AA}, shows a strong dependence on collision centrality but has weak dependence on Υ meson p_T and rapidity [108]. The forward rapidity ($2.5 \leq y^{\Upsilon} \leq 4.0$) measurement of the Υ suppression at ALICE [94] is found to be consistent with the midrapidity ($|y^{\Upsilon}| \leq 2.4$) measurement of the Υ suppression at the CMS. The CMS and ALICE collaborations have carried out the R_{AA} measurement of Υ at $\sqrt{s_{NN}} = 5.02$ TeV with the Run II LHC PbPb collisions [30, 104, 103]. The CMS experiment measured slightly more amount of Υ suppression at $\sqrt{s_{NN}} = 5.02$ TeV [30, 104] than the suppression at $\sqrt{s_{NN}} = 2.76$ TeV [108] while the ALICE experiment observed less suppression at $\sqrt{s_{NN}} = 5.02$ TeV than that at $\sqrt{s_{NN}} = 2.76$ TeV in the most central PbPb

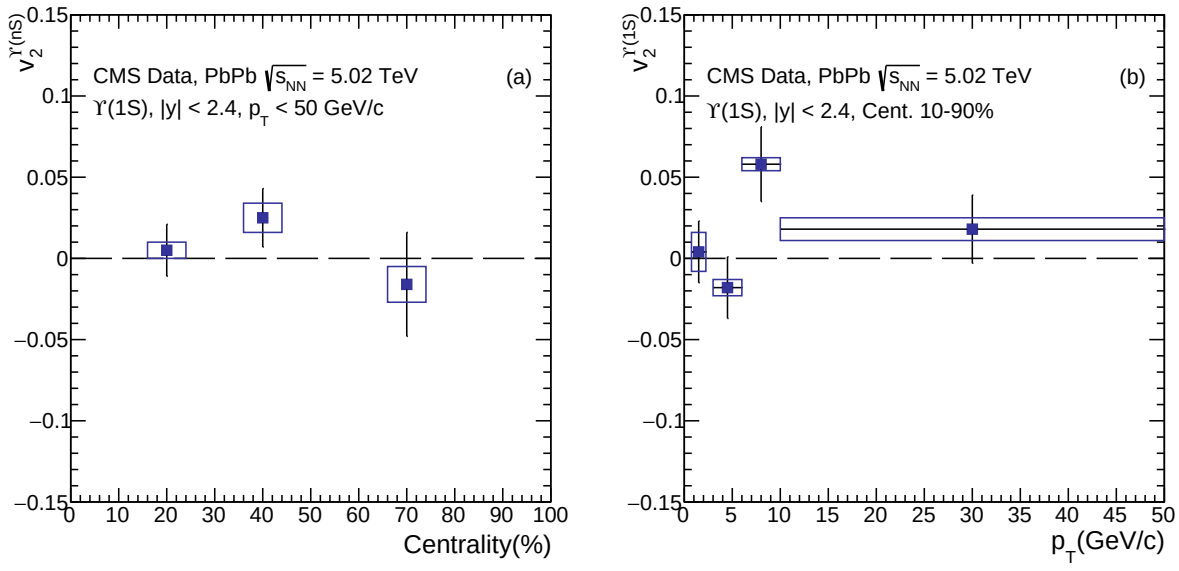

Figure 20: (Color online) The ϒ(1S) azimuthal anisotropy (v_2) (a) as a function of collision centrality and (b) as a function of transverse momentum p_T [109]. The vertical bars denote statistical uncertainties, and the rectangular boxes show the total systematic uncertainties.

collisions [94, 103].

3.4.2. ϒ(nS) azimuthal anisotropy at the LHC

The CMS experiment measured v_2 coefficients for ϒ(1S) and ϒ(2S) mesons in PbPb collisions at a nucleon-nucleon center-of-mass energy of 5.02TeV. Figure 20 shows the ϒ(1S) azimuthal anisotropy (v_2) (a) as a function of collision centrality and (b) as a function of transverse momentum p_T measured by CMS experiment at LHC [109]. The p_T integrated results shown in Fig. 20 (a) for three centrality intervals are consistent with zero within the statistical uncertainties. The average v_2 values in the 10-90% centrality interval measured by CMS experiment are found to be 0.007±0.011(stat)±0.005(syst) for ϒ(1S) and -0.063±0.085(stat)±0.037(syst) for ϒ(2S). The p_T dependence of ϒ(1S) meson v_2 values is measured for the 10-90% centrality interval. The v_2 values are consistent with zero in the measured p_T range, except for the $6<p_T<10$ GeV/c interval that shows a 2.6σ deviation from zero.

Figure 21 shows the p_T differential results for v_2 of ϒ(1S) mesons measured by CMS experiment along with the measurements of v_2 for ϒ(1S) and J/ψ from ALICE in the same p_T (0-15 GeV/c) and centrality (5-60%) interval. The measurements from CMS and ALICE are done in complementary rapidity ranges. The ϒ(1S) V_2 is consistant with zero while the J/ψ meson measured by ALICE in same kinematic conditions have finite v_2. Together, the CMS and ALICE results indicate that the geometry of the medium has little influence on the ϒ(1S) yields and recombination is not a dominant process in the production of this meson. The results also indicate that the path-length depen-dence of ϒ(1S) suppression is small.

Measurement by CMS and ATLAS.

3.4.3. ϒ(nS) R_{AA} at the RHIC

Measurement by STAR and PHENIX.

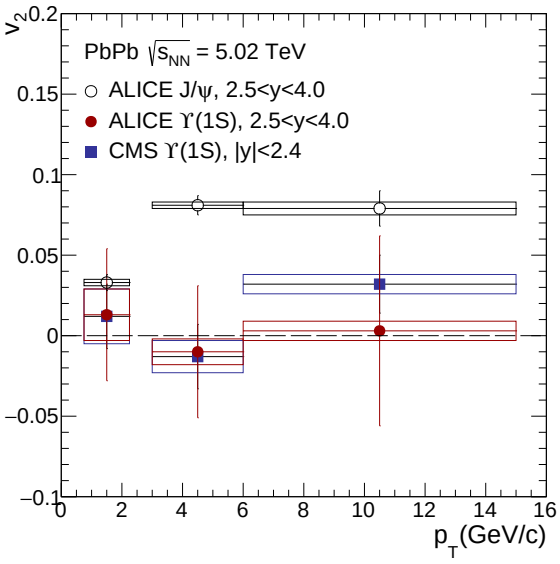

Figure 21: (Color online) The v_2 for Υ(1S) mesons as a function of p_T in the rapidity range —y—<2.4 measured by CMS experiment [109] compared with the ALICE results for $Upsilon$(1S) and J/ψ mesons measured in 2.5<y<4 [110]. The vertical bars denote statistical uncertainties, and the rectangular boxes show the total systematic uncertainties.

4. Conclusions and oulook

fgfghfhhhgh

[1] E. V. Shuryak, Quantum Chromodynamics and the Theory of Superdense Matter, Phys. Rept. 61 (1980) 71–158. doi:10.1016/0370-1573(80)90105-2.

[2] H. Satz, The Quark-Gluon Plasma: A Short Introduction, Nucl. Phys. A 862-863 (2011) 4–12. arXiv:1101.3937, doi:10.1016/j.nuclphysa.2011.05.014.

[3] H. Satz, Color deconfinement in nuclear collisions, Rept. Prog. Phys. 63 (2000) 1511. arXiv:hep-ph/0007069, doi:10.1088/0034-4885/63/9/203.

[4] T. Matsui, H. Satz, J/ψ Suppression by Quark-Gluon Plasma Formation, Phys. Lett. B 178 (1986) 416–422. doi:10.1016/0370-2693(86)91404-8.

[5] L. Kluberg, 20 years of J/psi suppression at the CERN SPS: Results from experiments NA38, NA51 and NA50, Eur. Phys. J. C 43 (2005) 145–156. doi:10.1140/epjc/s2005-02245-6.

[6] P. Nason, S. Dawson, R. K. Ellis, The Total Cross-Section for the Production of Heavy Quarks in Hadronic Collisions, Nucl. Phys. B 303 (1988) 607–633. doi:10.1016/0550-3213(88)90422-1.

[7] P. Nason, S. Dawson, R. K. Ellis, The One Particle Inclusive Differential Cross-Section for Heavy Quark Production in Hadronic Collisions, Nucl. Phys. B 327 (1989) 49–92, [Erratum: Nucl.Phys.B 335, 260–260 (1990)]. doi:10.1016/0550-3213(89)90286-1.

[8] G. T. Bodwin, E. Braaten, G. P. Lepage, Rigorous QCD analysis of inclusive annihilation and production of heavy quarkonium, Phys. Rev. D 51 (1995) 1125–1171, [Erratum: Phys.Rev.D 55, 5853 (1997)]. arXiv:hep-ph/9407339, doi:10.1103/PhysRevD.55.5853.

[9] N. Brambilla, et al., Heavy quarkonium physicsarXiv:hep-ph/0412158, doi:10.5170/CERN-2005-005.

[10] M. B. Einhorn, S. D. Ellis, Hadronic Production of the New Resonances: Probing Gluon Distributions, Phys. Rev. D 12 (1975) 2007. doi:10.1103/PhysRevD.12.2007.

[11] S. D. Ellis, M. B. Einhorn, C. Quigg, Comment on Hadronic Production of Psions, Phys. Rev. Lett. 36 (1976) 1263. doi:10.1103/PhysRevLett.36.1263.

[12] C. E. Carlson, R. Suaya, Hadronic Production of psi/J Mesons, Phys. Rev. D 14 (1976) 3115. doi:10.1103/PhysRevD.14.3115.

[13] E. L. Berger, D. L. Jones, Inelastic Photoproduction of J/psi and Upsilon by Gluons, Phys. Rev. D 23 (1981) 1521–1530. doi:10.1103/PhysRevD.23.1521.

[14] G. A. Schuler, Quarkonium production and decays, Ph.D. thesis, Hamburg U. (1994). arXiv:hep-ph/9403387.

[15] P. Artoisenet, J. P. Lansberg, F. Maltoni, Hadroproduction of J/ψ and Υ in association with a heavy-quark pair, Phys. Lett. B 653 (2007) 60–66. arXiv:hep-ph/0703129, doi:10.1016/j.physletb.2007.04.031.

[16] J. M. Campbell, F. Maltoni, F. Tramontano, QCD corrections to J/psi and Upsilon production at hadron colliders, Phys. Rev. Lett. 98 (2007) 252002. arXiv:hep-ph/0703113, doi:10.1103/PhysRevLett.98.252002.

[17] P. Artoisenet, J. M. Campbell, J. P. Lansberg, F. Maltoni, F. Tramontano, Υ Production at Fermilab Tevatron and LHC Energies, Phys. Rev. Lett. 101 (2008) 152001. arXiv:0806.3282, doi:10.1103/PhysRevLett.101.152001.

[18] H. Fritzsch, Producing Heavy Quark Flavors in Hadronic Collisions: A Test of Quantum Chromodynamics, Phys. Lett. B 67 (1977) 217–221. doi:10.1016/0370-2693(77)90108-3.

[19] J. F. Amundson, O. J. P. Eboli, E. M. Gregores, F. Halzen, Colorless states in perturbative QCD: Charmonium and rapidity gaps, Phys. Lett. B 372 (1996) 127–132. arXiv:hep-ph/9512248, doi:10.1016/0370-2693(96)00035-4.

[20] J. F. Amundson, O. J. P. Eboli, E. M. Gregores, F. Halzen, Quantitative tests of color evaporation: Charmonium production, Phys. Lett. B 390 (1997) 323–328. arXiv:hep-ph/9605295, doi:10.1016/S0370-2693(96)01417-7.

[21] H.-L. Lai, J. Guzzi, Marco an dHuston, Z. Li, P. M. Nadolsky, J. Pumplin, C. P. Yuan, New parton distributions for collider physics, Phys. Rev. DarXiv:1007.2241, doi:10.1103/PhysRevD.82.074024.

[22] R. E. Nelson, R. Vogt, A. D. Frawley, Narrowing the uncertainty on the total charm cross section and its effect on the J/ψ cross section, Phys. Rev. C 87 (1) (2013) 014908. arXiv:1210.4610, doi:10.1103/PhysRevC.87.014908.

[23] M. Cacciari, P. Nason, R. Vogt, QCD predictions for charm and bottom production at RHIC, Phys. Rev. Lett. 95 (2005) 122001. arXiv:hep-ph/0502203, doi:10.1103/PhysRevLett.95.122001.

[24] K. J. Eskola, H. Paukkunen, C. A. Salgado, EPS09: A New Generation of NLO and LO Nuclear Parton Distribution Functions, JHEP 04 (2009) 065. arXiv:0902.4154, doi:10.1088/1126-6708/2009/04/065.

[25] V. Kumar, P. Shukla, R. Vogt, Components of the dilepton continuum in Pb+Pb collisions at $\sqrt{s_{NN}} = 2.76$ TeV, Phys. Rev. C 86 (2012) 054907. arXiv:1205.3860, doi:10.1103/PhysRevC.86.054907.

[26] S. Chatrchyan, et al., Observation and studies of jet quenching in PbPb collisions at nucleon-nucleon center-of-mass energy = 2.76 TeV, Phys. Rev. C 84 (2011) 024906. arXiv:1102.1957, doi:10.1103/PhysRevC.84.024906.

[27] B. Povh, K. Rith, C. Scholz, F. Zersche, W. Rodejohann, Particles and nuclei: An Introduction to the physical concepts, Graduate Texts in Physics, Springer, 1995. doi:10.1007/3-540-36684-9.

[28] S. M. Ikhdair, R. Sever, A Systematic study on nonrelativistic quarkonium interaction, Int. J. Mod. Phys. A 21 (2006) 3989–4002. arXiv:hep-ph/0508144, doi:10.1142/S0217751X06030953.

[29] A. M. Sirunyan, et al., Measurement of prompt and nonprompt charmonium suppression in PbPb collisions at 5.02 TeV, Eur. Phys. J. C 78 (6) (2018) 509. arXiv:1712.08959, doi:10.1140/epjc/s10052-018-5950-6.

[30] A. M. Sirunyan, et al., Measurement of nuclear modification factors of Υ(1S), Υ(2S), and Υ(3S) mesons in PbPb collisions at $\sqrt{s_{\mathrm{NN}}} = 5.02$ TeV, Phys. Lett. B 790 (2019) 270–293. arXiv:1805.09215, doi:10.1016/j.physletb.2019.01.006.

[31] S. Acharya, et al., Studies of J/ψ production at forward rapidity in Pb-Pb collisions at $\sqrt{s_{\mathrm{NN}}}$ = 5.02 TeV, JHEP 02 (2020) 041. arXiv:1909.03158, doi:10.1007/JHEP02(2020)041.

[32] S. Acharya, et al., Υ suppression at forward rapidity in Pb-Pb collisions at $\sqrt{s_{\mathrm{NN}}}$ = 5.02 TeV, Phys. Lett. B 790 (2019) 89–101. arXiv:1805.04387, doi:10.1016/j.physletb.2018.11.067.

[33] M. Strickland, Thermal υ_{1s} and chi_b1 suppression in $\sqrt{s_{NN}} = 2.76$ TeV Pb-Pb collisions at the LHC, Phys. Rev. Lett. 107 (2011) 132301. arXiv:1106.2571, doi:10.1103/PhysRevLett.107.132301.

[34] T. Song, K. C. Han, C. M. Ko, Bottomonia suppression in heavy-ion collisions, Phys. Rev. C 85 (2012) 014902. arXiv:1109.6691, doi:10.1103/PhysRevC.85.014902.

[35] V. Kumar, P. Shukla, R. Vogt, Quarkonia suppression in PbPb collisions at $\sqrt{s_{NN}}$ = 2.76 TeV, Phys. Rev. C 92 (2) (2015) 024908. arXiv:1410.3299, doi:10.1103/PhysRevC.92.024908.

[36] V. Kumar, P. Shukla, A. Bhattacharyya, Suppression of quarkonia in PbPb collisions at $\sqrt{s_{NN}} = 5.02$ TeV, J. Phys. G 47 (1) (2020) 015104. arXiv:1909.10785, doi:10.1088/1361-6471/ab51cf.

[37] N. Brambilla, et al., QCD and Strongly Coupled Gauge Theories: Challenges and Perspectives, Eur. Phys. J. C 74 (10) (2014) 2981. arXiv:1404.3723, doi:10.1140/epjc/s10052-014-2981-5.

[38] J. L. Domenech, M. A. Sanchis-Lozano, Bottomonium production at the Tevatron and the LHC, Phys. Lett. B 476 (2000) 65–72. arXiv:hep-ph/9911332, doi:10.1016/S0370-2693(00)00119-2.

[39] J. L. Domenech, M. A. Sanchis-Lozano, Results from bottomonia production at the Tevatron and prospects for the LHC, Nucl. Phys. B 601 (2001) 395–421. arXiv:hep-ph/0012296, doi:10.1016/S0550-3213(01)00053-0.

[40] B. Gong, J.-X. Wang, H.-F. Zhang, QCD corrections to Υ production via color-octet states at the Tevatron and LHC, Phys. Rev. D 83 (2011) 114021. arXiv:1009.3839, doi:10.1103/PhysRevD.83.114021.

[41] R. Sharma, I. Vitev, High transverse momentum quarkonium production and dissociation in heavy ion collisions, Phys. Rev. C 87 (4) (2013) 044905. arXiv:1203.0329, doi:10.1103/PhysRevC.87.044905.

[42] P. Sun, C. P. Yuan, F. Yuan, Heavy Quarkonium Production at Low Pt in NRQCD with Soft Gluon Resummation, Phys. Rev. D 88 (2013) 054008. arXiv:1210.3432, doi:10.1103/PhysRevD.88.054008.

[43] B. Gong, L.-P. Wan, J.-X. Wang, H.-F. Zhang, Complete next-to-leading-order study on the yield and polarization of $\Upsilon(1S, 2S, 3S)$ at the Tevatron and LHC, Phys. Rev. Lett. 112 (3) (2014) 032001. arXiv:1305.0748, doi:10.1103/PhysRevLett.112.032001.

[44] Y. Feng, B. Gong, L.-P. Wan, J.-X. Wang, An updated study of Υ production and polarization at the Tevatron and LHC, Chin. Phys. C 39 (12) (2015) 123102. arXiv:1503.08439, doi:10.1088/1674-1137/39/12/123102.

[45] H. Han, Y.-Q. Ma, C. Meng, H.-S. Shao, Y.-J. Zhang, K.-T. Chao, $\Upsilon(nS)$ and $\chi_b(nP)$ production at hadron colliders in nonrelativistic QCD, Phys. Rev. D 94 (1) (2016) 014028. arXiv:1410.8537, doi:10.1103/PhysRevD.94.014028.

[46] G.-M. Yu, Y.-B. Cai, Y.-D. Li, J.-S. Wang, Heavy quarkonium photoproduction in ultrarelativistic heavy ion collisions, Phys. Rev. C 95 (1) (2017) 014905, [Addendum: Phys.Rev.C 95, 069901 (2017)]. arXiv:1703.03194, doi:10.1103/PhysRevC.95.014905.

[47] D. Acosta, et al., Υ Production and Polarization in $p\bar{p}$ Collisions at $\sqrt{s} = 1.8$-TeV, Phys. Rev. Lett. 88 (2002) 161802. doi:10.1103/PhysRevLett.88.161802.

[48] R. Aaij, et al., Measurement of Upsilon production in pp collisions at $\sqrt{s}$ = 7 TeV, Eur. Phys. J. C 72 (2012) 2025. arXiv:1202.6579, doi:10.1140/epjc/s10052-012-2025-y.

[49] V. Khachatryan, et al., Measurements of the Υ(1S), Υ(2S), and Υ(3S) differential cross sections in pp collisions at $\sqrt{s} = 7$ TeV, Phys. Lett. B 749 (2015) 14–34. arXiv:1501.07750, doi:10.1016/j.physletb.2015.07.037.

[50] G. Aad, et al., Measurement of Upsilon production in 7 TeV pp collisions at ATLAS, Phys. Rev. D 87 (5) (2013) 052004. arXiv:1211.7255, doi:10.1103/PhysRevD.87.052004.

[51] S. Chatrchyan, et al., Measurement of the $\Upsilon(1S)$, $\Upsilon(2S)$, and $\Upsilon(3S)$ Cross Sections in pp Collisions at $\sqrt{s}$ = 7 TeV, Phys. Lett. B 727 (2013) 101–125. arXiv:1303.5900, doi:10.1016/j.physletb.2013.10.033.

[52] A. M. Sirunyan, et al., Measurement of quarkonium production cross sections in pp collisions at $\sqrt{s} = 13$ TeV, Phys. Lett. B 780 (2018) 251–272. arXiv:1710.11002, doi:10.1016/j.physletb.2018.02.033.

[53] P. A. Zyla, et al., Review of Particle Physics, PTEP 2020 (8) (2020) 083C01. doi:10.1093/ptep/ptaa104.

[54] V. Kumar, P. Shukla, Charmonia production in p + p collisions under NRQCD formalism, J. Phys. G 44 (8) (2017) 085003. arXiv:1606.08265, doi:10.1088/1361-6471/aa7818.

[55] R. Baier, R. Ruckl, Hadronic Collisions: A Quarkonium Factory, Z. Phys. C 19 (1983) 251. doi:10.1007/BF01572254.

[56] B. Humpert, NARROW HEAVY RESONANCE PRODUCTION BY GLUONS, Phys. Lett. B 184 (1987) 105–107. doi:10.1016/0370-2693(87)90496-5.

[57] R. Gastmans, W. Troost, T. T. Wu, Production of Heavy Quarkonia From Gluons, Nucl. Phys. B 291 (1987) 731. doi:10.1016/0550-3213(87)90493-7.

[58] P. L. Cho, A. K. Leibovich, Color octet quarkonia production, Phys. Rev. D 53 (1996) 150–162. arXiv:hep-ph/9505329, doi:10.1103/PhysRevD.53.150.

[59] P. L. Cho, A. K. Leibovich, Color octet quarkonia production. 2., Phys. Rev. D 53 (1996) 6203–6217. arXiv:hep-ph/9511315, doi:10.1103/PhysRevD.53.6203.

[60] T.-J. Hou, et al., New CTEQ global analysis of quantum chromodynamics with high-precision data from the LHC, Phys. Rev. D 103 (1) (2021) 014013. arXiv:1912.10053, doi:10.1103/PhysRevD.103.014013.

[61] S. Digal, P. Petreczky, H. Satz, Quarkonium feed-down and sequential suppression, Phys. Rev. D 64 (2001) 094015. arXiv:0106017.

[62] T. Umeda, K. Nomura, H. Matsufuru, Charmonium at finite temperature in quenched lattice QCD , Eur. Phys. J. C 39S1 (2005) 9. arXiv:0211003.

[63] M. Asakawa, T. Hatsuda, J/ψ and η_C in the deconfined plasma from lattice QCD arXiv:0308034.

[64] S. Datta, F. Karsch, P. Petreczky, I. Wetzorke, Behavior of charmonium systems after deconfinement , Phys. Rev. D 69 (2004) 094507. arXiv:0312037.

[65] A. Jakovác, P. Petreczky, K. Petrov, A. Velytsky, Quarkonium correlators and spectral functions at zero and finite temperature, Phys. Rev. D 75 (2007) 014506. arXiv:0611017.

[66] C. Allton, M. B. Oktay, M. Peardon, J. Skullerud, Charmonium at high temperature in two-flavor QCD, Phys. Rev. D 76 (2007) 094513. arXiv:0705.2198.

[67] C. Y. Wong, Heavy quarkonia in quark gluon plasma, Phys. Rev. C 72 (2005) 034906.

[68] A. Mócsy, P. Petreczky, Quarkonia correlators above deconfinement, Phys. Rev. D 73 (2006) 074007. arXiv:0512156.

[69] A. Mócsy, P. Petreczky, Heavy quarkonia survival in potential model, Eur. Phys. J. C 43 (2005) 77. arXiv:0411262.

[70] W. M. Alberico, A. Beraudo, A. D. Pace, A. Molinari, , Phys. Rev. D. 76 (2007) 114506.

[71] D. Cabrera, R. Rapp, T-matrix approach to quarkonium correlation functions in the QGP, Phys. Rev. D 76 (2007) 114506. arXiv:0611134.

[72] A. Mócsy, P. Petreczky, Can quarkonia survive deconfinement ? , Phys. Rev. D 77 (2008) 014501. arXiv:0705.2559.

[73] A. Mócsy, P. Petreczky, Color Screening Melts Quarkonium, Phys. Rev. Lett. 99 (2007) 211602. arXiv:0705.2183.

[74] M. Laine, O. Philipsen, M. Tassler, Thermal imaginary part of a real-time static potential from classical lattice gauge theory simulations, JHEP 0709 (2007) 066. arXiv:0707.2458.

[75] M. Laine, A resummed perturbative estimate for the quarkonium spectral function in hot QCD , JHEP 0705 (2007) 028. arXiv:0704.1720.

[76] M. Laine, How to compute the thermal quarkonium spectral function from first principles?, Nucl. Phys. A 820 (2009) 25C. arXiv:0801.1112.

[77] N. Brambilla, J. Ghiglieri, A. Vairo, P. Petreczky, Static quark-antiquark pairs at finite temperature, Phys. Rev. D 78 (2008) 014017. arXiv:0804.0993.

[78] P. Petreczky, Recent progress in lattice QCD at finite temperaturearXiv:0906.0502.

[79] P. Petreczky, Quarkonium in Hot Medium, J. Phys. G. 37 (2010) 094009. arXiv:1001.5284.

[80] O. Kaczmarek, F. Karsch, P. Petreczky, F. Zantow, Heavy Quark Anti-Quark Free Energy and the Renormalized Polyakov Loop, Phys. Lett. B 543 (2002) 41. arXiv:0207002.

[81] C. Lourenco, R. Vogt, H. K. Woehri, Energy dependence of J/psi absorption in proton-nucleus collisions, JHEP 02 (2009) 014. arXiv:0901.3054, doi:10.1088/1126-6708/2009/02/014.

[82] R. L. Thews, M. Schroedter, J. Rafelski, Enhanced J/ψ production in deconfined quark matter, Phys. Rev. C 63 (2001) 054905. arXiv:hep-ph/0007323, doi:10.1103/PhysRevC.63.054905.

[83] X. Zhao, R. Rapp, Medium Modifications and Production of Charmonia at LHC, Nucl. Phys. A 859 (2011) 114–125. arXiv:1102.2194, doi:10.1016/j.nuclphysa.2011.05.001.

[84] P. Huovinen, P. Petreczky, QCD Equation of State and Hadron Resonance Gas, Nucl. Phys. A 837 (2010) 26–53. arXiv:0912.2541, doi:10.1016/j.nuclphysa.2010.02.015.

[85] K. Aamodt, et al., Centrality dependence of the charged-particle multiplicity density at mid-rapidity in Pb-Pb collisions at $\sqrt{s_{NN}} = 2.76$ TeV, Phys. Rev. Lett. 106 (2011) 032301. arXiv:1012.1657, doi:10.1103/PhysRevLett.106.032301.

[86] S. Chatrchyan, et al., Dependence on pseudorapidity and centrality of charged hadron production in PbPb collisions at a nucleon-nucleon centre-of-mass energy of 2.76 TeV, JHEP 08 (2011) 141. arXiv:1107.4800, doi:10.1007/JHEP08(2011)141.

[87] E. V. Shuryak, Two stage equilibration in high-energy heavy ion collisions, Phys. Rev. Lett. 68 (1992) 3270–3272. doi:10.1103/PhysRevLett.68.3270.

[88] E. Abbas, et al., Centrality dependence of the pseudorapidity density distribution for charged particles in Pb-Pb collisions at $\sqrt{s_{\rm NN}}$ = 2.76 TeV, Phys. Lett. B 726 (2013) 610–622. arXiv:1304.0347, doi:10.1016/j.physletb.2013.09.022.

[89] G. Bhanot, M. E. Peskin, Short Distance Analysis for Heavy Quark Systems. 2. Applications, Nucl. Phys. B 156 (1979) 391–416. doi:10.1016/0550-3213(79)90200-1.

[90] F. Karsch, M. T. Mehr, H. Satz, Color Screening and Deconfinement for Bound States of Heavy Quarks, Z. Phys. C 37 (1988) 617. doi:10.1007/BF01549722.

[91] F. Arleo, P. B. Gossiaux, T. Gousset, J. Aichelin, Heavy quarkonium hadron cross-section in QCD at leading twist, Phys. Rev. D 65 (2002) 014005. arXiv:hep-ph/0102095, doi:10.1103/PhysRevD.65.014005.

[92] R. L. Thews, M. L. Mangano, Momentum spectra of charmonium produced in a quark-gluon plasma, Phys. Rev. C 73 (2006) 014904. arXiv:nucl-th/0505055, doi:10.1103/PhysRevC.73.014904.

[93] S. Chatrchyan, et al., Observation of Sequential Upsilon Suppression in PbPb Collisions, Phys. Rev. Lett. 109 (2012) 222301, [Erratum: Phys.Rev.Lett. 120, 199903 (2018)]. arXiv:1208.2826, doi:10.1103/PhysRevLett.109.222301.

[94] B. B. Abelev, et al., Suppression of $\Upsilon(1S)$ at forward rapidity in Pb-Pb collisions at $\sqrt{s_{\rm NN}} = 2.76$ TeV, Phys. Lett. B 738 (2014) 361–372. arXiv:1405.4493, doi:10.1016/j.physletb.2014.10.001.

[95] T. Affolder, et al., Production of $\Upsilon(1S)$ mesons from χ_b decays in $p\bar{p}$ collisions at $\sqrt{s} = 1.8$ TeV, Phys. Rev. Lett. 84 (2000) 2094–2099. arXiv:hep-ex/9910025, doi:10.1103/PhysRevLett.84.2094.

[96] M. Strickland, D. Bazow, Thermal Bottomonium Suppression at RHIC and LHC, Nucl. Phys. A 879 (2012) 25–58. arXiv:1112.2761, doi:10.1016/j.nuclphysa.2012.02.003.

[97] A. Dumitru, Y. Guo, M. Strickland, , Phys. Lett. B 662 (2009) 37.

[98] O. Kaczmarek, F. Karsch, F. Zantow, P. Petreczky, , Phys. Rev. D 70 (2004) 074505.

[99] G. S. Bali, K. Schilling, A. Wachter, , Physical. Rev. D 56 (1997) 2566.

[100] R. Vogt, M. Prakash, P. Koch, T. H. Hansson, J/ψ Interactions With Hot Hadronic Matter, Phys. Lett. B 207 (1988) 263–268. doi:10.1016/0370-2693(88)90572-2.

[101] M. Gluck, E. Reya, A. Vogt, Pionic parton distributions, Z. Phys. C 53 (1992) 651–656. doi:10.1007/BF01559743.

[102] S. Chatrchyan, et al., Indications of suppression of excited Υ states in PbPb collisions at $\sqrt{S_{NN}}$ = 2.76 TeV, Phys. Rev. Lett. 107 (2011) 052302. arXiv:1105.4894, doi:10.1103/PhysRevLett.107.052302.

[103] S. Acharya, et al., Υ suppression at forward rapidity in Pb-Pb collisions at $\sqrt{s_{\rm NN}}$ = 5.02 TeV, Phys. Lett. B 790 (2019) 89–101. arXiv:1805.04387, doi:10.1016/j.physletb.2018.11.067.

[104] A. M. Sirunyan, et al., Suppression of Excited Υ States Relative to the Ground State in Pb-Pb Collisions at $\sqrt{s_{\rm NN}}$=5.02 TeV, Phys. Rev. Lett. 120 (14) (2018) 142301. arXiv:1706.05984, doi:10.1103/PhysRevLett.120.142301.

[105] L. Adamczyk, et al., Suppression of Υ production in d+Au and Au+Au collisions at $\sqrt{s_{NN}}$=200 GeV, Phys. Lett. B 735 (2014) 127–137, [Erratum: Phys.Lett.B 743, 537–541 (2015)]. arXiv:1312.3675, doi:10.1016/j.physletb.2014.06.028.

[106] L. He, T. Edmonds, Z.-W. Lin, F. Liu, D. Molnar, F. Wang, Anisotropic parton escape is the dominant source of azimuthal anisotropy in transport models, Phys. Lett. B 753 (2016) 506–510. arXiv:1502.05572, doi:10.1016/j.physletb.2015.12.051.

[107] S. Voloshin, Y. Zhang, Flow study in relativistic nuclear collisions by Fourier expansion of Azimuthal particle distributions, Z. Phys. C 70 (1996) 665–672. arXiv:hep-ph/9407282, doi:10.1007/s002880050141.

[108] V. Khachatryan, et al., Suppression of $\Upsilon(1S)$, $\Upsilon(2S)$ and $\Upsilon(3S)$ production in PbPb collisions at $\sqrt{s_{\rm NN}}$ = 2.76 TeV, Phys. Lett. B 770 (2017) 357–379. arXiv:1611.01510, doi:10.1016/j.physletb.2017.04.031.

[109] A. M. Sirunyan, et al., Measurement of the azimuthal anisotropy of Υ(1S) and Υ(1S) mesons in PbPb collisions at $\sqrt{s_{\mathrm{NN}}} = 5.02$ TeV, Phys. Lett. B 819 (2021) 136385. arXiv:2006.07707, doi:10.1016/j.physletb.2021.136385.

[110] S. Acharya, et al., Measurement of $\Upsilon(1\mathrm{S})$ elliptic flow at forward rapidity in Pb-Pb collisions at $\sqrt{s_{\mathrm{NN}}} = 5.02$ TeV, Phys. Rev. Lett. 123 (19) (2019) 192301. arXiv:1907.03169, doi:10.1103/PhysRevLett.123.192301.